Table 3 Summary of the expression profiles of selected genes determined by RT-PCR

Gene/lineage	34^-KSL	SP-KSL	34^+KSL	Lin^-	Ter119	Mac-1	Gr-1	B220
Expression of all six genes identified as in common among SCDb, $CD34^-$KSL, and SP Lin^- libraries								
Gfi1b	+++	+++	++	+	++	−	−	±
3110045G13Rik	±	+++	+	−	−	−	−	−
Mfng	++	++	−	−	−	−	−	+
Rgs18	+++	±	+	++	−	±	−	−
Exosc2	±	±	±	±	±	−	−	±
Serpina3g	++	++	+	±	−	−	−	±
Expression of seven selected genes identified as in common only between $CD34^-$KSL and SP Lin^- libraries								
Armcx	+++	++	+	+	−	−	±	−
BC28440	+++	+++	++	+	±	−	±	+
D11Erf416e	+	+	±	++	−	−	−	±
1110019N10Rik	++	+	+	++	±	±	±	++
2810405O22Rik	++	++	++	++	++	±	++−	++
Bre	++	+++	+	+++	+++	+	+	+++
Calcrl	±	+	++	+	+++	±	−	±

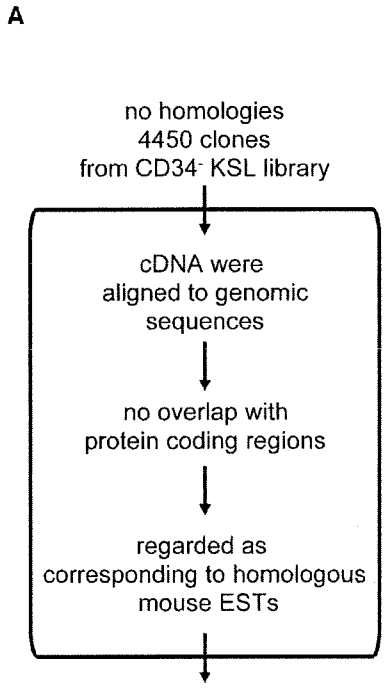

B

Chromosome No.	Clone No.	Accession No.
Chr 1	1	CN539228
Chr 1	1	AA596108
Chr 2	4	CX236158
Chr 3	4	CK795576
Chr 3	1	BE740716
Chr 4	1	CN697221
Chr 4	1	BB578787
Chr 4	2	CB598798
Chr 4	9	CB847565
Chr 4	1	BE534564
Chr 5	1	BQ892059
Chr 5	1	CX235980
Chr 5	1	BB683661
Chr 5	1	BP771729
Chr 6	1	CX220266
Chr 6	1	BX517570
Chr 6	8	CB849402
Chr 6	2	BU924501
Chr 8	1	BX528492
Chr 9	5	AU021499
Chr 11	1	CA881051
Chr 11	1	BQ567063
Chr 11	1	CK129343
Chr 11	1	CK377676
Chr 16	1	CA885675
Chr 17	2	BB661487
Chr 17	4	BM241006
Chr 17	1	BY722123
Chr 19	1	BE200491

Fig. 6 Identification of putative mRNA-like non-coding RNAs. **a** Scheme of the computational screening of non-coding RNA candidates. **b** List of non-coding RNA candidates. Chromosomal location, number of clones identified, and accession number of each candidate are indicated

coding RNAs. Further characterization of identified HSC-specific genes and their products, particularly with regard to their functional aspects in HSCs, will be highly helpful in elucidating the molecular mechanisms of HSC regulation.

References

1. Osawa M, Hanada K, Hamada H, Nakauchi H. Long-term lymphohematopoietic reconstitution by a single CD34-low/negative hematopoietic stem cell. Science. 1996;273:242–5.
2. Goodell MA, Brose K, Paradis G, Conner AS, Mulligan RC. Isolation and functional properties of murine hematopoietic stem cells that are replicating in vivo. J Exp Med. 1996;183:1797–806.
3. Zhou S, Schuetz JD, Bunting KD, Colapietro AM, Sampath J, Morris JJ, et al. The ABC transporter Bcrp1/ABCG2 is expressed in a wide variety of stem cells and is a molecular determinant of the side-population phenotype. Nat Med. 2001;7:1028–34.
4. Bertoncello I, Hodgson GS, Bradley TR. Multiparameter analysis of transplantable hemopoietic stem cells: I. The separation and enrichment of stem cells homing to marrow and spleen on the basis of rhodamine-123 fluorescence. Exp Hematol. 1985;13:999–1006.
5. Spangrude GJ, Heimfeld S, Weissman IL. Purification and characterization of mouse hematopoietic stem cells. Science. 1988;241:58–62.
6. Uchida N, Weissman IL. Searching for hematopoietic stem cells: evidence that Thy-1.1lo Lin- Sca-1+ cells are the only stem cells in C57BL/Ka-Thy-1.1 bone marrow. J Exp Med. 1992;175:175–84.
7. Jordan CT, Astle CM, Zawadzki J, Mackarehtschian K, Lemischka IR, Harrison DE. Long-term repopulating abilities of enriched fetal liver stem cells measured by competitive repopulation. Exp Hematol. 1995;23:1011–5.
8. Terskikh AV, Easterday MC, Li L, Hood L, Kornblum HI, Geschwind DH, et al. From hematopoiesis to neuropoiesis: evidence of overlapping genetic programs. Proc Natl Acad Sci USA. 2001;98:7934–9.
9. Park IK, He Y, Lin F, Laerum OD, Tian Q, Bumgarner R, et al. Differential gene expression profiling of adult murine hematopoietic stem cells. Blood. 2002;99:488–98.
10. Venezia TA, Merchant AA, Ramos CA, Whitehouse NL, Young AS, Shaw CA, et al. Molecular signatures of proliferation and quiescence in hematopoietic stem cells. PLoS Biol. 2004;2(10):e301. doi:10.1371/journal.pbio.0020301.
11. Phillips RL, Ernst RE, Brunk B, Ivanova N, Mahan MA, Deanehan JK, et al. The genetic program of hematopoietic stem cells. Science. 2000;288:1635–40.
12. Ivanova NB, Dimos JT, Schaniel C, Hackney JA, Moore KA, Lemischka IR. A stem cell molecular signature. Science. 2002;298:601–4.
13. Chambers SM, Boles NC, Lin KY, Tierney MP, Bowman TV, Bradfute SB, et al. Hematopoietic fingerprints: an expression database of stem cells and their progeny. Cell Stem Cell. 2007;1:578–91.
14. Kitamura T, Koshino Y, Shibata F, Oki T, Nakajima H, Nosaka T, et al. Retrovirus-mediated gene transfer and expression cloning: powerful tools in functional genomics. Exp Hematol. 2003;31:1007–14.
15. Altschul SF, Gish W, Miller W, Myers EW, Lipman DJ. Basic local alignment search tool. J Mol Biol. 1990;215:403–10.
16. Ashburner M, Ball CA, Blake JA, Botstein D, Butler H, Cherry JM, et al. Gene ontology: tool for the unification of biology. The gene ontology consortium. Nat Genet. 2000;25:25–9.
17. Osawa M, Yamaguchi T, Nakamura Y, Kaneko S, Onodera M, Sawada K, et al. Erythroid expansion mediated by the Gfi-1B zinc finger protein: role in normal hematopoiesis. Blood. 2002;100:2769–77.
18. Chen CZ, Li L, Lodish HF, Bartel DP. MicroRNAs modulate hematopoietic lineage differentiation. Science. 2004;303:83–6.
19. Wagner LA, Christensen CJ, Dunn DM, Spangrude GJ, Georgelas A, Kelley L, et al. EGO, a novel, noncoding RNA gene, regulates eosinophil granule protein transcript expression. Blood. 2007;109:5191–8.
20. Akashi K, He X, Chen J, Iwasaki H, Niu C, Steenhard B, et al. Transcriptional accessibility for genes of multiple tissues and hematopoietic lineages is hierarchically controlled during early hematopoiesis. Blood. 2003;101:383–9.
21. Ramalho-Santos M, Yoon S, Matsuzaki Y, Mulligan RC, Melton DA. "Stemness": transcriptional profiling of embryonic and adult stem cells. Science. 2002;298:597–600.
22. Okazaki Y, Furuno M, Kasukawa T, Adachi J, Bono H, Kondo S, et al. Analysis of the mouse transcriptome based on functional annotation of 60, 770 full-length cDNAs. Nature. 2002;420:563–73.
23. Numata K, Kanai A, Saito R, Kondo S, Adachi J, Wilming KG, et al. Identification of putative noncoding RNAs among the RIKEN mouse full-length cDNA collection. Genome Res. 2003;13:1301–6.
24. Simin K, Scuderi A, Reamey J, Dunn S, Weiss R, Metherall JE, et al. Profiling patterned transcripts in Drosophila embryos. Genome Res. 2002;12:1040–7.
25. Barciszewski J, Vrdmann VA. Noncoding RNAs: molecular biology and molecular medicine. Georgetown, TX/New York, NY. Landes Bioscience/Eurekah.com; Kluwer Academic/Plenum Publishers; 2003.
26. Brockdorff N, Ashworth A, Kay GF, Cooper P, Smith S, McCabe VM, et al. Conservation of position and exclusive expression of mouse Xist from the inactive X chromosome. Nature. 1991;351:329–31.

Identification of cancer stem cells in a Tax-transgenic (Tax-Tg) mouse model of adult T-cell leukemia/lymphoma

*Jumpei Yamazaki,[1,2] *Takuo Mizukami,[1] Kazuya Takizawa,[1] Madoka Kuramitsu,[1] Haruka Momose,[1] Atsuko Masumi,[1] Yasushi Ami,[3] Hideki Hasegawa,[4] William W. Hall,[5] Hajime Tsujimoto,[2] Isao Hamaguchi,[1] and Kazunari Yamaguchi[1]

[1]Department of Safety Research on Blood and Biologics, National Institute of Infectious Diseases, Tokyo, Japan; [2]Veterinary Internal Medicine, University of Tokyo, Tokyo, Japan; Departments of [3]Animal Science and [4]Pathology, National Institute of Infectious Diseases, Tokyo, Japan; and [5]Centre for Research in Infectious Diseases, School of Medicine & Medical Science, University College Dublin, Dublin, Republic of Ireland

Adult T-cell leukemia/lymphoma (ATL) is a malignant lymphoproliferative disorder caused by HTLV-I infection. In ATL, chemotherapeutic responses are generally poor, which has suggested the existence of chemotherapy-resistant cancer stem cells (CSCs). To identify CSC candidates in ATL, we have focused on a Tax transgenic mouse (Tax-Tg) model, which reproduces ATL-like disease both in Tax-Tg animals and also after transfer of Tax-Tg splenic lymphomatous cells (SLCs) to nonobese diabetic/severe combined immunodeficiency (NOD/SCID) mice. Using a limiting dilution transplantation, it was estimated that one CSC existed per 10^4 SLCs (0.01%). In agreement with this, we have successfully identified candidate CSCs in a side population (0.06%), which overlapped with a minor population of $CD38^-/CD71^-/CD117^+$ cells (0.03%). Whereas lymphoma did not develop after transplantation of 10^2 SLCs, 10^2 CSCs could consistently regenerate the original lymphoma. In addition, lymphoma and CSCs could also be demonstrated in the bone marrow and $CD117^+$ CSCs were observed in both osteoblastic and vascular niches. In the CSCs, *Tax*, *Notch1*, and *Bmi1* expression was down-regulated, suggesting that the CSCs were derived from Pro-T cells or early hematopoietic progenitor cells. Taken together, our data demonstrate that CSCs certainly exist and have the potential to regenerate lymphoma in our mouse model. (Blood. 2009;114:2709-2720)

Introduction

Adult T-cell leukemia-lymphoma (ATL) is an aggressive and clonal lymphoproliferative disorder of mature T cells caused by infection with human T-lymphotropic virus type I (HTLV-1).[1] An estimated 10 million to 20 million people are infected with HTLV-1 globally, and infection is endemic in southwestern Japan, Africa, the Caribbean basin, and South America.[2] Although the majority of infected persons remain clinically asymptomatic, approximately 6.6% of males and 2.1% of females will develop ATL. In Japan, 1.2 million persons are infected with HTLV-1, and 800 to 1000 new ATL cases develop each year. ATL has been divided into 4 subtypes: chronic, smoldering, acute, and lymphoma-type.[3] Acute and lymphoma-type have an aggressive clinical course with lymphadenopathy, hepatosplenomegaly, visceral invasion by malignant cells, and the appearance of leukemic cells with multilobulated nuclei termed "flower cells" in peripheral blood. The most common cell phenotype in ATL is $CD2^+$, $CD3^+$, $CD4^+$, $CD8^-$, and $CD25^+$. Other phenotypes, which include $CD4^-/CD8^-$ double-negative (DN), $CD8^+$, and $CD4^+/CD8^+$ double-positive, occur more rarely.[4] FOXP3 (forkhead box P3) expression, which is predominantly expressed in $CD4^+/CD25^+$ regulatory T cells (Tregs), has also been detected in some ATL cases, suggesting that disease may originate in Treg cells.[5] In addition, HTLV-I can also infect human hematopoietic progenitor cells and immature thymocytes, which would also account for the range of phenotypes observed.[6]

Studies have shown that initiation of oncogenesis is triggered by the viral Tax protein. Tax interacts with the nuclear factor-κB (NF-κB)–Rel signaling complex and activates NF-κB, which results in the up-regulation of various cytokines and their receptor genes, and alterations in cell signaling and cell-cycle regulation.[7] Recent studies have clearly demonstrated the oncogenic properties of Tax in vivo. Specifically, transgenic animals with Tax expression restricted to developing thymocytes developed an ATL-like phenotype and leukemogenesis developed in both immature[8] and mature T cells.[9] The treatment of ATL is unsatisfactory. Various combination chemotherapy regimens have produced poor outcomes; however, intensive induction therapy (interferon-α and zidovudine) has produced significant complete remission rates in certain cases.[10,11] Unfortunately, most patients relapse, and this has been considered to be the result of the existence of cancer stem cells (CSCs) similar to what has been described both in other types of leukemia and solid tumors. Specifically, CSCs have been identified in malignancies of both hematopoietic origin[12,13] and in breast, brain, prostate, colon, and pancreatic carcinomas.[14] CSCs have the potential to self-renew, develop inherent drug-resistance, and can regenerate the original tumors when transplanted into severe combined immunocompromised nonobese diabetic/severe combined immunodeficiency (NOD/SCID) mice.[15] As a consequence, CSCs are considered important targets for anticancer therapy.[16]

To identify and confirm the existence of CSCs in ATL, we have focused our initial studies on an HTLV-Tax transgenic mouse (Tax-Tg) model,[8] where transgene expression was controlled by the LCK promoter, which limits transgene expression to developing thymocytes. The clinical, pathologic, and immunologic features observed in this Tax-Tg model are similar to those observed in the

Submitted August 17, 2008; accepted May 28, 2009. Prepublished online as *Blood* First Edition paper, July 7, 2009; DOI 10.1182/blood-2008-08-174425.

An Inside *Blood* analysis of this article appears at the front of this issue.

*J.Y. and T.M. contributed equally to this study.

The publication costs of this article were defrayed in part by page charge payment. Therefore, and solely to indicate this fact, this article is hereby marked "advertisement" in accordance with 18 USC section 1734.

aggressive forms of human ATL. Lymphoma and leukemia develop at 10 to 23 months, which is equivalent to human disease (20-60 years) and is characterized by the widespread distribution of lymphomatous cells in various organs and the presence of flower cells in peripheral blood. Lymphomatous cells displayed a $CD4^-CD8^-$ DN phenotype. In addition, lymphomas could be regenerated in NOD/SCID mice after transplantation of Tax-Tg splenic lymphomatous cells. In this study, we have successfully identified candidate CSCs using xenografting into NOD/SCID mouse and flow cytometric analysis. Specifically, we identified CSCs in a side population (SP; 0.06%), which overlapped with a minor population of $CD38^-/CD71^-/CD117^+$ cells (0.03%). Using the NOD/SCID transplantation assay, we found that 10^2 CSCs could regenerate the original lymphoma. This is first report describing a CSC candidate in an ATL model, and we think that similar studies will inform and may ultimately allow the identification of CSCs in human disease.

Methods

Animal models of ATL

Animal experiments were approved by the Animal Care and Use Committee of the National Institute of Infectious Disease, Tokyo, Japan. For transplantation studies, we obtained NOD/SCID mice (NOD.CB17-Prkdc^{scid}/J) 6 to 12 weeks of age from The Jackson Laboratory, and these were housed under constant temperature and light.

Transplantation assays

ATL-like lymphoma and leukemia was first established in NOD/SCID mice by intraperitoneal injection of 10^5 frozen stock Tax transgenic (Tax-Tg) splenic lymphomatous cells (SLCs). After 40 days, ATL-like lymphoma developed in the NOD/SCID mouse spleen, and SLCs could regenerate the original ATL-like lymphoma when further injected. Using this NOD/SCID mouse transplantation system, SLCs could be serially passed as required. We used 4th-passage frozen stocked SLCs for the serial transplantation studies. We performed 3 consecutive serial transplantations by intraperitoneal injection of 10^5 SLCs (first transplantation [n = 12], second transplantation [n = 5], third transplantation [n = 7]). We also performed limiting dilution assays by intraperitoneal injection of 10^6 (n = 5), 10^5 (n = 4), 10^4 (n = 3), 10^3 (n = 5), and 10^2 (n = 7) of freshly isolated SLCs. To evaluate the lymphoma-forming ability of CSC candidates, we also transplanted 10^2 CSCs ($CD38^-/CD71^-/CD117^+$; n = 9), non-CSC fraction ($CD38^+/CD71^+/CD117^-$; n = 11), and SLCs (n = 11) into NOD/SCID mice.

Flow cytometry and SP analysis

To identify candidate CSCs in the SLCs, we performed SP cell analysis. SLCs were suspended in Hanks balanced salt solution medium (Invitrogen) containing 2% fetal bovine serum, 10 mM N-2-hydroxyethylpiperazine-N′-2-ethanesulfonic acid buffer (Invitrogen), and incubated with Hoechst 33342 dye (2.5 μg/mL, Invitrogen, H-3570) with or without verapamil (Sigma-Aldrich) at 37°C for 60 minutes, according to the method outlined by Goodell et al.[17] After staining with or without Hoechst 33342, the cells were stained with phycoerythrin (PE) anti–mouse/rat Foxp3 (clone FJK-16s), PE anti–mouse CD3e (145-2C11), PE anti–mouse CD8 (53-6.7), PE anti–mouse CD127 (clone A7R34), PE anti–mouse CD38 (clone 90), fluorescein isothiocyanate (FITC) anti–mouse Sca-1 (clone D7), FITC anti–mouse CD2 (RM2-5), FITC anti–mouse CD4 (RM4-5), FITC anti–mouse CD123 (clone 5B11), FITC anti–mouse CD24 (clone 30-F1), FITC anti–mouse CD71 (clone R17217), and allophycocyanin (APC) anti–mouse CD25 (clone PC61.5), APC anti–mouse CD133 (clone 13A4), APC anti–mouse CD117(clone ACK2), APC anti–mouse CD25 (PC61.5), and purified anti–mouse CD44 (IM7) at 4°C for 30 minutes and then counterstained with 2 μg/mL propidium iodide (BD Biosciences). All antibodies were obtained from eBioscience. We performed flow-cytometric analysis and cell sorting using JSAN (Bay Bioscience) with 350-nm UV laser for SP analysis. Cytospin preparations of the sorted cells were prepared and subjected to Wright/Giemsa staining.

Histologic preparation and periodic acid-Schiff–hematoxylin staining

NOD/SCID mouse spleen, bone marrow (BM), liver, lung, lymph node, and epidermal tissues were harvested and fixed in Bouin solution (Sigma-Aldrich) or 4% (wt/vol) paraformaldehyde in phosphate-buffered saline (pH 7.5) at 4°C for 24 hours. After fixation, samples were dehydrated in a graded ethanol series and cleared in xylene, and then embedded in paraffin; 4-μm semithin sections were prepared using a carbon steel blade (Feather Safety Razor Co) by microtome (Yamato Kouki). Tissue sections were mounted on super-frosted glass slides coated with methyl-amino-silane (Matsunami Glass). To identify periodic acid-Schiff (PAS)–positive ATL leukemia/lymphoma[18] in spleen, we performed PAS-hematoxylin staining as previously described.[19] Histologic images were aqquired using a NikonEclipse E1000 microscope equipped with 10×/0.30, 20×/0.50, 40×/0.75, and 100×/1.30 NA objective lenses. Images were captured with a Nikon DXM 1200F digital camera.

Immunohistochemistry

Anti–mouse CD3 antibody (ab5690; Abcam), anti–mouse CD44 (IM7; BioLegend), anti–mouse/human CD117 (C-19; Santa Cruz Biotechnology), and anti–mouse CD4 (RM4-5; eBioscience) were used as primary antibodies, and biotinylated goat anti–rat IgG-B (SC-2041, Santa Cruz Biotechnology) and biotinylated goat anti–rabbit IgG-B (SC-2040, Santa Cruz Biotechnology) were used as secondary antibodies. Staining was carried out as previously described.[20] Briefly, after blocking with 3% bovine serum albumin (BSA) in phosphate-buffered saline, sections (4-μm thick) were incubated with anti-CD3, -CD4, -CD44, and -CD117 antibody (each diluted 1:200) at 4°C overnight. Signals were detected using a Vectastain ABC Elite Kit (Vector Laboratories), and nuclei were stained with Gill III-hematoxylin.

Quantitative analysis of gene expression

Poly (A)+ RNAs were extracted from 5×10^3 candidate CSCs ($CD38^-/CD71^-/CD117^+$) and non-CSCs ($CD38^+/CD71^+/CD117^-$) using a Micro-Fast Track 2.0 Kit (Invitrogen), and cDNAs were prepared using SMART polymerase chain reaction (PCR) cDNA synthesis kits (Clontech) as previously described.[20] Real-time PCR reactions were performed using SYBR PreMix ExTaq (Takara Shuzo) and a Light Cycler (Roche Diagnostics). The primer pairs used in this study were *Notch1* (5′-CGTGGTCTTCAAGCGTGATG-3′ and 5′-AGCTCTTCCTCGTGGCCATA-3′), *CD44* (5′-AGCTGACGAGACCCGGAAT-3′ and 5′-CGTAGGCACTACACCCCAATC-3′), *Rex1* (5′-TGTGCTGCCTCCAAGTGTTG-3′ and 5′-ATCCGCAAACACCTGCTTTT-3′), and *N-cadherin* (5′-CACAGCCACAGCCGTCATC-3′ and 5′-GCAGTAAACTCTGGAGGATTGTCA-3′) and for *Tax*,[8] *CD117*, *Bmi1*, *SCL/tal-1*, and *β-actin* as previously described.[20] *β-Actin* was used as an internal control. Real-time PCR was carried out using 40 cycles at 94.0°C for 1 minute, 60°C for 25 seconds (2-step). Amplification of predicted fragments was confirmed by melt-curve analysis and gel electrophoresis. To determine the relative amounts of product, we used the comparative threshold cycle method, according to the manufacturer's instructions (Roche Diagnostics). Expression levels are reported relative to mouse *β-actin*.

Genomic DNA isolation and PCR assays for Tax transgene integration mapping

Genomic DNA was extracted from 5×10^6 splenic and BM mononuclear cells using the DNeasy Blood & Tissue Kit system (QIAGEN). Cells were isolated from NOD/SCID mice with or without transplantation of Tax-Tg-derived SLCs. All genomic DNAs were treated with RNase A (100 mg/mL).

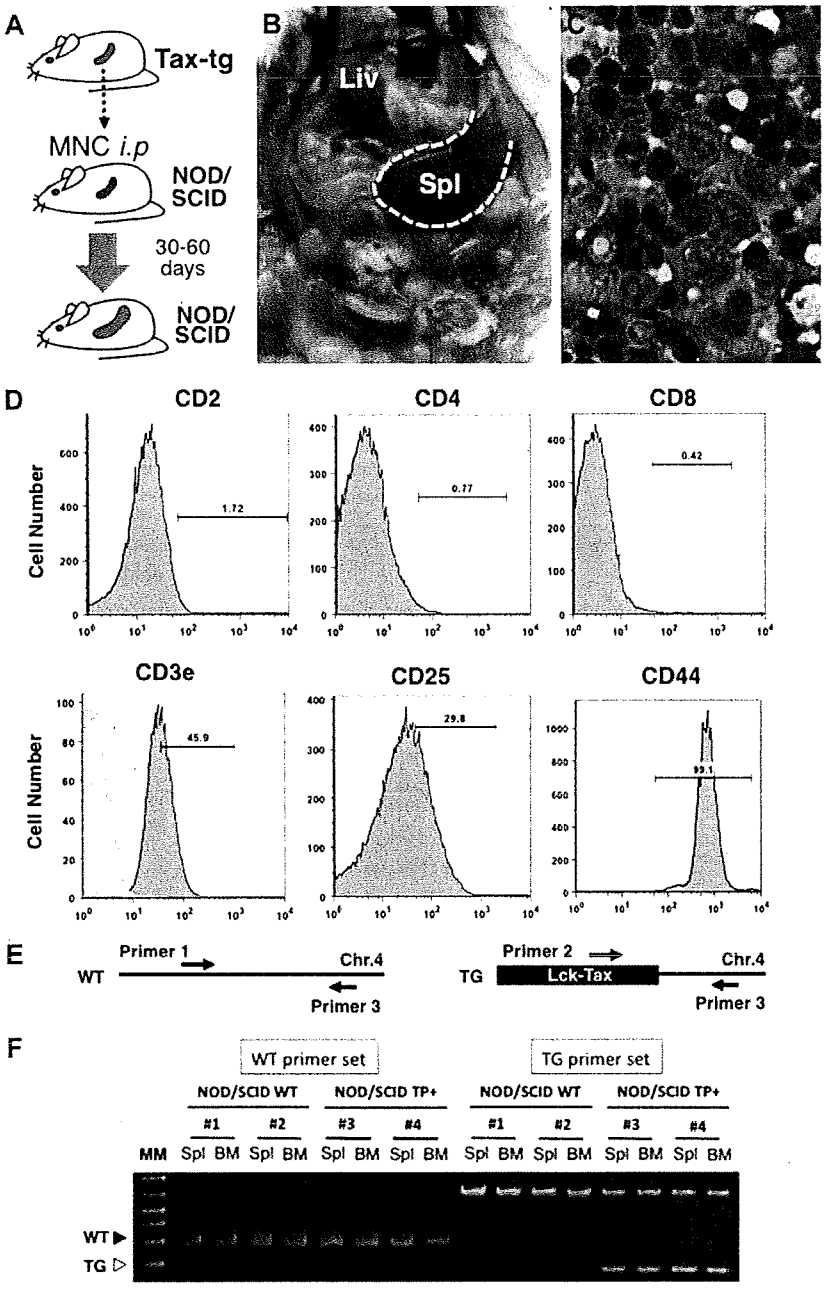

Figure 1. Transplantation of Tax-Tg mouse-derived splenic mononuclear cells to NOD/SCID mice. (A) Experimental design of the transplantation assay. (B) Remarkable splenomegaly was observed in the lymphoma-reconstituted NOD/SCID mouse. Spl indicates spleen; and Liv, liver. The dotted line shows the outline of the enlarged spleen. (C) Cytospin analysis of spleen cells isolated from reconstituted lymphoma in the NOD/SCID mouse. The spleen was filled with ATL-like lymphomatous cells. (D) Surface marker analysis of lymphomatous cells from spleen. These had the identical phenotype of lymphomatous cell reconstituted by Tax-Tg–derived splenic mononuclear cells: $CD2^-$, $CD4^-$, $CD8^-$, cytoplasmic $CD3^+$, and surface $CD25^+$ and $CD44^+$. (E) Schematic representation of the PCR assay to identify and confirm the Tax transgenic integration site. Lck-Tax transgenes were tandemly inserted on the chromosome 4 (Chr.4) in the original transgenic animals. (F) Genotyping of mononuclear cells in the spleen and BM. WT PCR product (300 bp) was detected in both the normal and CSC-transplanted NOD/SCID spleen and BM. However, Tax-Tg (TG) PCR products identifying the expected integration site of the transgene (200 bp) were detected only in the reconstituted ATL-like lymphomatous cells in spleen and BM. TP+ indicates transplantation.

PCR primers were constructed based on the integration site of Tax gene on chromosome 4 in the Tax-Tg mouse model.[8] The primers used to detect the Tax-Tg or wild-type (WT) NOD/SCID mouse derived genomic DNA were NOD/SCID mouse (5′-TGT TGC ATA CAG GAA GCC CA-3′ and 5′-GCG GTA CAG TGT GTG CTT TGA G-3′) and Tax-Tg (5′-GAC ACA GCA TAG GCT ACC TGG C-3′ and 5′-GCG GTA CAG TGT GTG CTT TGA G-3′; Figure 1E). PCR reactions were performed using ExTaq (Takara Shuzo) and a Thermal Cycler (Bio-Rad). The PCR was carried out using 95°C for 2 minutes, 40 cycles at 94.0°C for 30 seconds, 58°C for 30 seconds, and 72°C for 30 seconds. The PCR products were analyzed by electrophoresis on 2% agarose gels.

Data analysis

Significant differences were calculated using the Student *t* test for gene expression analysis. Statistical analyses were performed using GraphPad Prism (Version 5, GraphPad Software) and Excel 2008 (Microsoft Japan).

Results

Lymphoma/leukemia regenerative activity in the Tax-Tg mouse and SLCs

Hasegawa et al reported that Tax-Tg SLCs could regenerate ATL-like lymphoma when transplanted into NOD/SCID mice and that Tax-Tg SLCs had the potential to regenerate the original lymphoma when further transplanted in NOD/SCID mice.[8] To assess the stem cell potential within the SLCs, we performed serial transplantation experiments by intraperitoneal injections of frozen stocked 4th-passed 10^5 SLCs into NOD/SCID mice (Figure 1A). SLCs could regenerate original lymphoma and leukemia in the first transplantation (12 of 12 animals) with the development of marked

splenomegaly (Figure 1B-C) and BM involvement resulting from infiltration of malignant cells. The phenotypes of the SLCs were similar to the original tumors in Tax-Tg animals. Surface staining for CD2, CD4, and CD8 was negative, but cytoplasmic CD3 and surface CD25 and CD44 were positive in the SLCs (Figure 1D). SLCs could regenerate original lymphoma and leukemia after second (5 of 5 animals) and third transplantation (6 of 7 animals) by day 40.

To confirm that the SLCs were derived from the original leukemic cells, we performed PCR analysis to confirm the Tax transgenic integration site. In the Tax-Tg model, the transgene was found to be integrated in the A9 region of chromosome 4. PCR analysis with amplification across the integration site demonstrated that this was identical in the lymphomatous cells arising in both spleen and BM (Figure 1E-F), confirming that they were derived from the original leukemic cells and that variant populations had not arisen nor were selected. These studies provided functional evidence for self-renewal and supported the existence of CSCs, which have leukemia/lymphoma regenerative potential, within the SLCs.

Identification of CSCs in SLCs by surface marker analysis

It has been suggested that CSCs are a small and minor population in both leukemias[12,13] and solid tumors.[14] To identify the candidate CSC populations in SLCs, we performed detailed cell surface marker analysis, to investigate phenotypic expression patterns previously observed in Tregs (CD25, CD127, FoxP3), hematopoietic stem cells (HSCs; CD117, CD34, CD38, Sca-1, c-kit), and markers previously identified in other CSCs (CD71, CD123, CD24, CD90, CD133). Surface marker analyses are shown in Figure 2A through D. Expression patterns were divided into 4 profiles: partial and low expression; CD127, CD117, CD123, FoxP3, CD133, CD90, and CD34 (Figure 2B); heterogeneous expression; CD71 and CD25 (Figure 2C); and major expression; CD38, CD24, and Sca-1 (Figure 2D).

Certain cases of human ATL are thought to originate from Tregs, which express CD4, $CD25^{int\text{-}hi}$, FOXP3,[21] and CD127.[22] Whereas Foxp3 expression was not detected (0.03%) in the SLCs, CD25 expression was heterogeneously detected (64.5%) and CD127 expression was detected at low levels (1.17%; Figure 2B-C). Recent studies have shown that leukemia stem cells can share HSC properties ($CD34^+/CD38^-$ cells), and it could also be shown that these could regenerate the original disease in NOD/SCID mice.[23] In the mouse, HSCs are enriched in $CD34^-/c\text{-}kit^+/Sca\text{-}1^+/Lineage^-$ cell population.[24] CD34 and CD117 (c-kit) expression in the SLCs was partially detected (0.63% and 0.56%). CD38 and Sca-1 highly expressed at 94.3% and 89.9%, respectively (Figure 2B,D). We also examined expression of CD123 (IL-3Ra), which is a well-established marker for leukemia stem cells,[12] CD133, which is a common CSC marker found in brain,[25] and colon cancer,[26] CD24, which has been identified in prostate CSCs,[27] and CD90, which is associated with CSCs in non-small-cell lung carcinoma.[28] In the SLCs, expression of CD71 and CD24 were 52.2% and 92.7%, respectively. In contrast, the expression of CD123, CD90, and CD133 was only detected at low levels, 0.13%, 0.89%, and 0.3%, respectively (Figure 2B-D).

Next, we performed multiple stainings for the identification of small populations within the SLCs (Table 1), and we successfully identified such a population, which was $CD38^-/CD71^-$. With a combination of CD117, we successfully confirmed the existence of a minor population (0.03%), which was $CD38^-/CD71^-/CD117^+$ (Figure 2E). In contrast, $CD38^-/CD71^-/CD133^+$ cells were not detected in SLCs (0%).

Identification of candidate CSCs for functional studies

Recent studies have shown that SPs are enriched for CSCs in various types of malignancies.[29] The SP phenotype is based on the ability of the cells to efficiently reflux the Hoechst 33342 fluorescent staining dye through the multidrug ABC transporter (ABCG2), and this property allows the isolation of the cells using flow cytometry. It is also considered that efflux efficiency in CSCs correlates with anticancer drug resistance and recurrence of disease after chemotherapy. To identify candidate CSCs, we investigated the SPs by evaluating efficient efflux of Hoechst 33342 dye in the SLCs. We successfully identified a small population (0.06%) corresponding to SP cells in the SLCs (Figure 3A); correspondingly, the SP fraction disappeared with treatment with the ABC transporter inhibitor verapamil. To further characterize the SP cells, we performed combination SP and surface marker analysis, and it could be shown that more than 50% of $CD38^-/CD71^-/CD117^+$ cells overlapped with the SP fraction in the SLCs (Figure 3B), suggesting that the CSC candidate(s) were associated with these populations.

The candidate CSC cells were also sorted for morphologic studies (Figure 3C). Isolated $CD38^-/CD71^-/CD117^+$ cells were blastoid cells and had scanty cytoplasm with no granules (Figure 3D). In contrast, $CD38^+/CD71^+/CD117^-$ cells were slightly larger and lymphocyte-like with dispersed chromatin and an irregularly shaped and prominent nucleus (Figure 3E).

In vivo lymphoma reconstitution assay of candidate CSCs

We performed transplantation analysis to assess the functionality of the candidate CSCs using the NOD/SCID mouse model. In initial studies, we performed limiting dilution analysis to estimate the frequency of the CSCs in the SLCs. We transplanted 10^6, 10^5, 10^4, 10^3, and 10^2 SLCs into NOD/SCID mice. It has been previously demonstrated that 10^5 SLCs could regenerate original leukemia and lymphoma observed in the Tax-Tg mice,[8] and this was evident by marked splenomegaly and confirmed by cytology at 40 days after transplantation. Spleen weights were approximately 10- to 20-fold larger than nontreated NOD/SCID mouse spleen (data not shown). In addition to the development of lymphoma, ascites also developed in the NOD/SCID mice. Using these criteria, we evaluated the lymphoma-regenerative activity in the candidate CSC and non-CSC fractions (Table 2). Whereas 10^2 SLCs could not regenerate original lymphoma and leukemia (0%) in the NOD/SCID mouse, 10^4 SLCs could, as expected, regenerate the original lymphoma and leukemia in all animals (100%). Lymphoma and leukemia after transplantation of 10^3 SLCs developed in 20% of animals. These results suggested that one CSC existed in 10^4 SLCs (0.01%), and indeed this frequency estimate was consistent with our surface marker and SP analysis studies.

We then isolated CSCs from SLCs, and 10^2 CSCs were transplanted into NOD/SCID mouse. At 40 days after transplantation, lymphoma and leukemia formation was not observed in 6 of the CSC transplanted NOD/SCID mice examined. However, at 60 days after transplantation, ATL-like lymphoma was observed in all 9 of the 9 CSC-injected NOD/SCID mice. All developed typical splenomegaly (Figure 4A-B) and ascites (Figure 4C). Total spleen

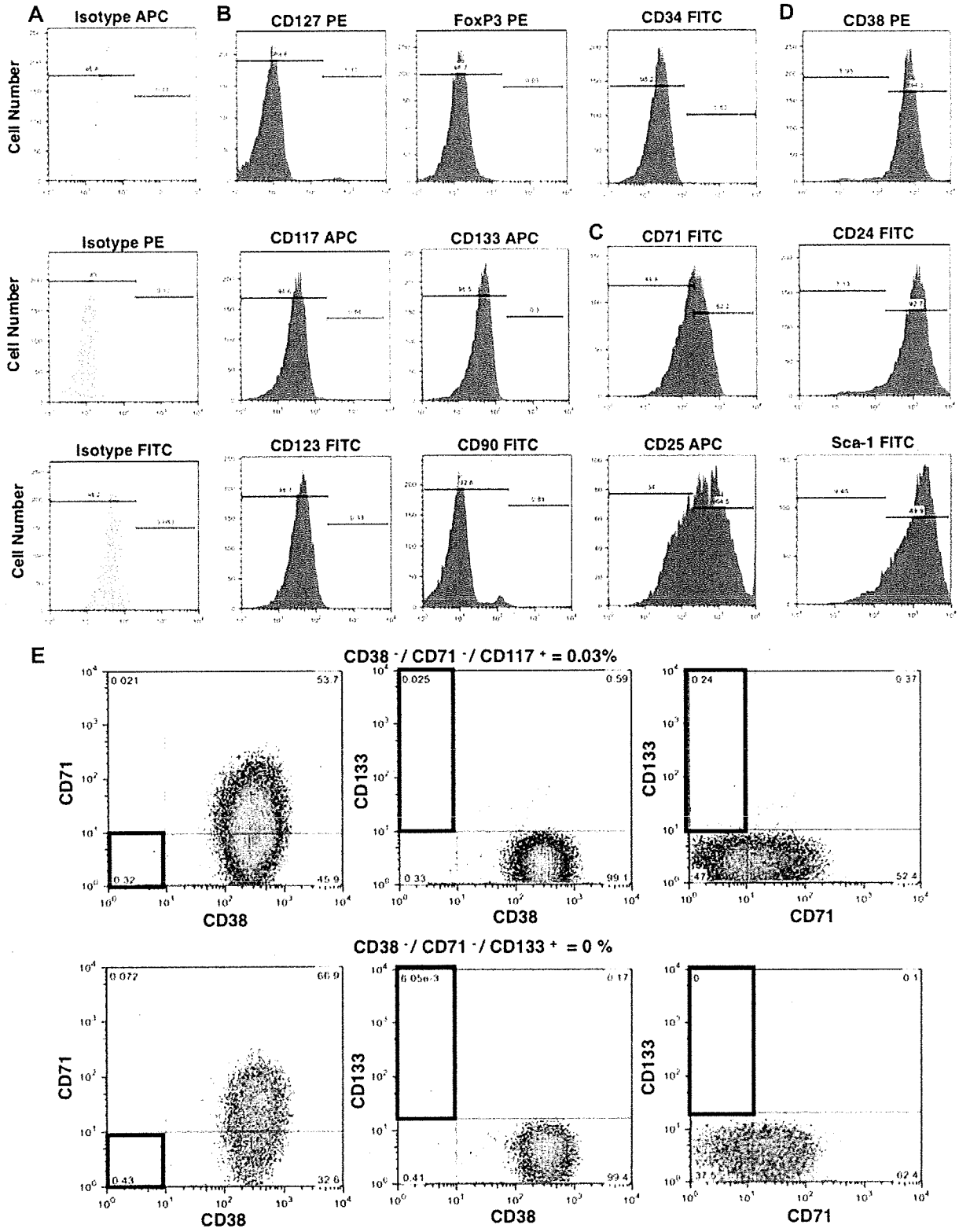

Figure 2. Flow cytometric analysis of NOD/SCID repopulating ATL-like lymphoma cells. Lymphoma and leukemia were generated in NOD/SCID mice by the transplantation of frozen stocked 4th-passage Tax-Tg SLCs. SLCs were isolated from spleen. (A) Histograms of isotype APC, PE, and FITC markers as controls. Expression profiles were divided into 4 patterns: partial and low, heterogeneous, and major types. (B) Partial and low expression: CD127, CD117, CD123, FoxP3, CD133, CD90, and CD34 are expressed at low levels in SLCs. (C) Heterogeneous expression: CD71 and CD25 are heterogeneously expressed in SLCs. (D) Major: CD38, CD24, and Sca-1 are highly expressed in SLCs. The percentage of individual subpopulations was determined according to isotype control in each assay. Dead cells were gated out by propidium iodide. (E) Triple-staining analysis with CD38, CD71, and CD117 or CD133 in the SLCs. $CD38^-/CD71^-/CD117^+$ cells were 0.03% and $CD38^-/CD71^-/CD133^+$ cells were 0% of total SLCs.

Table 1. Surface marker analysis of the NOD/SCID repopulating ATL-like lymphoma cells

Phenotype	Frequency (%)
CD38⁻/CD71⁻/CD117⁺	0.03-0.05
CD38⁻/CD71⁻/CD133⁺	0
CD38⁻/CD71⁻	0.3-0.5
CD38⁻/CD117⁺	0.10
CD71⁻/CD117⁺	0.15
CD38⁻/CD133⁺	< 0.01
CD71⁻/CD133⁺	< 0.01
Side population cells*	0.03-0.06
Aldehyde dehydrogenase activity*	0

Summary of surface marker combination analysis of ATL-like lymphoma cells in the NOD/SCID mouse. CD38⁻/CD71⁻/CD117⁺ cells were overlapped with side population cells.

*Functional assay.

weight was significantly increased only in the CSC-transplanted-NOD/SCID mouse spleen (Figure 4D). No lymphoma was observed after transplantation of 10^2 SLCs (n = 11) and the non-CSC fraction (CD38⁺/CD71⁺/CD117⁻ : n = 11) at 60 days. Analysis of the splenic cells isolated from 10^2 CSC-transplanted NOD/SCID mouse showed similar profiles to the first transplantation experiment using 10^5 SLCs, in that they were CD25⁺/CD44⁺ (data not shown) and contained SP cells (0.06%; Figure 4E) and the CSC-associated (CD38⁻/CD71⁻/CD117⁺) cell population (Figure 4F). These results clearly show that within this cell population are CSCs in that they have the SP phenotype and have the potential for self-renewal and the ability to regenerate the original lymphoma and leukemia.

Histologic analysis of spleen, BM, and other tissues

To confirm and characterize in more detail the lymphoma and leukemia in spleen after transplantation with the candidate CSCs,

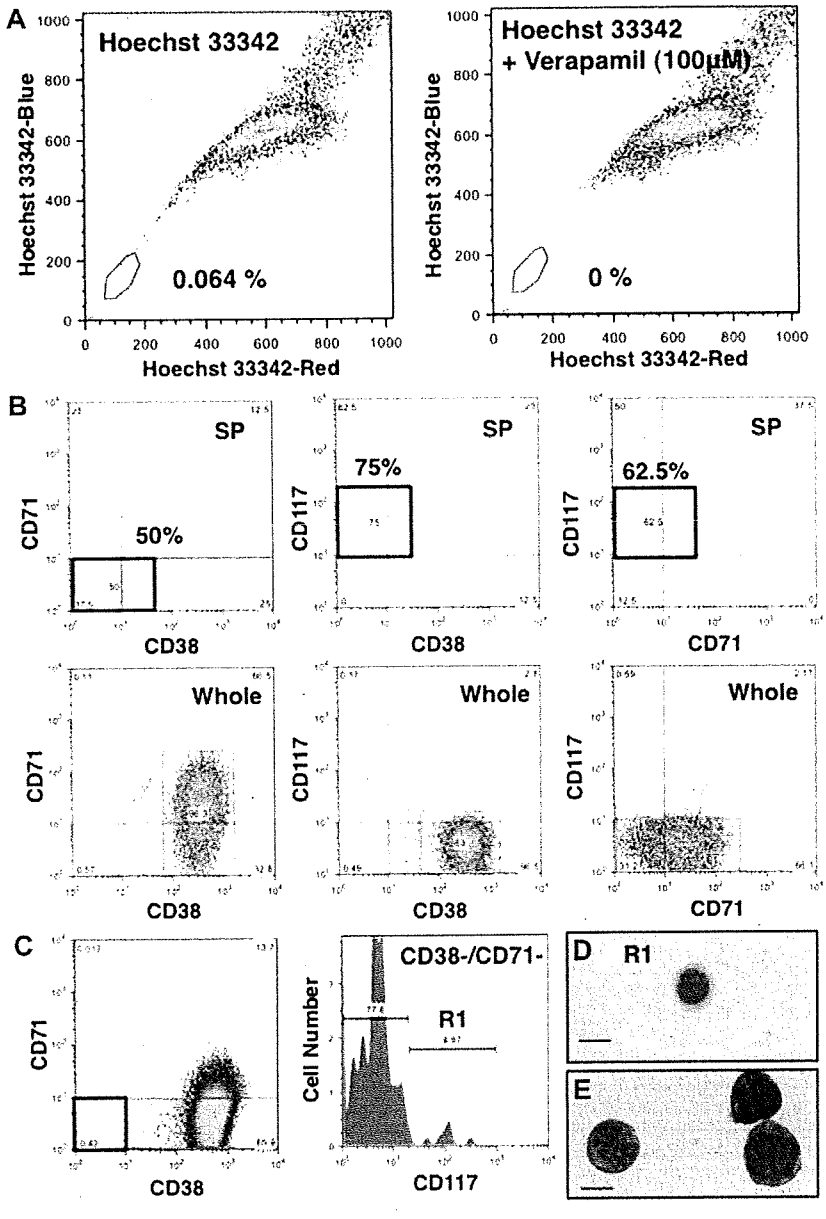

Figure 3. Functional analysis in the NOD/SCID repopulating ATL-like lymphoma cells. (A) SP cell analysis in the NOD/SCID repopulating ATL-like lymphoma cells. The SP regions are indicated by a trapezoid on each panel. (Left panel) Approximately 0.064% of SP cells were observed in the SLCs. (Right panel) SP cell analysis after treatment with verapamil (100 μM), where the SP fraction was lost. (B) Triple-staining analysis of CD38, CD71, and CD117 in the SP fraction. More than 50% of CD38⁻/CD71⁻/CD117⁺ corresponded to the SP fraction. (C) FACS CD38⁻/CD71⁻/CD117⁺ and CD38⁻/CD71⁻/CD117⁻ cells. (D) Cytospin analysis of the CSC candidate (CD38⁻/CD71⁻/CD117⁺) and (E) non-CSC candidate (CD38⁺/CD71⁺/CD117⁻) populations.

Table 2. Limiting dilution analysis in assessing stem cell activity

No. of cells	SLCs	CSCs ($CD38^-/CD71^-/CD117^+$)	Non-CSCs ($CD38^+/CD71^+/CD117^-$)
Short-term incubation (40 days)			
10^6	5/5	NT	NT
10^5	3/4	NT	NT
10^4	3/3	NT	NT
10^3	1/5	NT	NT
10^2	0/7	0/6	NT
Long-term incubation (60 days)			
10^2	0/11	9/9	0/11

Assessment of stem cell activity in the ATL-like lymphoma cell using limiting dilution assay of transplantation cells. One CSC was thought to exist in 10^4 SLCs. At long-term incubation, only CSC fractions can repopulate and regenerate original ATL-like lymphoma in the NOD/SCID mouse.

NT indicates no transplantation.

we performed histologic and immunohistochemical analyses. It has been reported that ATL leukemic cells have abundant PAS-strong positive cytoplasmic inclusions.[18] We could show that PAS-hematoxylin strong positive staining was only observed in lymphoma and leukemia in spleens after transplantation with 10^5 SLCs and 10^2 CSCs (Figure 5A-B). PAS-strong positive cells were not identified in the spleen after transplantation with 10^2 non-CSCs and SLCs (Figure 5C). To confirm the existence of malignant cells, we performed immunohistochemistry for CD3, CD4, CD44, and CD117. $CD3^+$ leukemic cells were observed only in the splenic lymphoma after transplantation of 10^2 CSCs and 10^5 SLCs. No $CD4^+$ cells were observed in the CSCs and non-CSC–transplanted

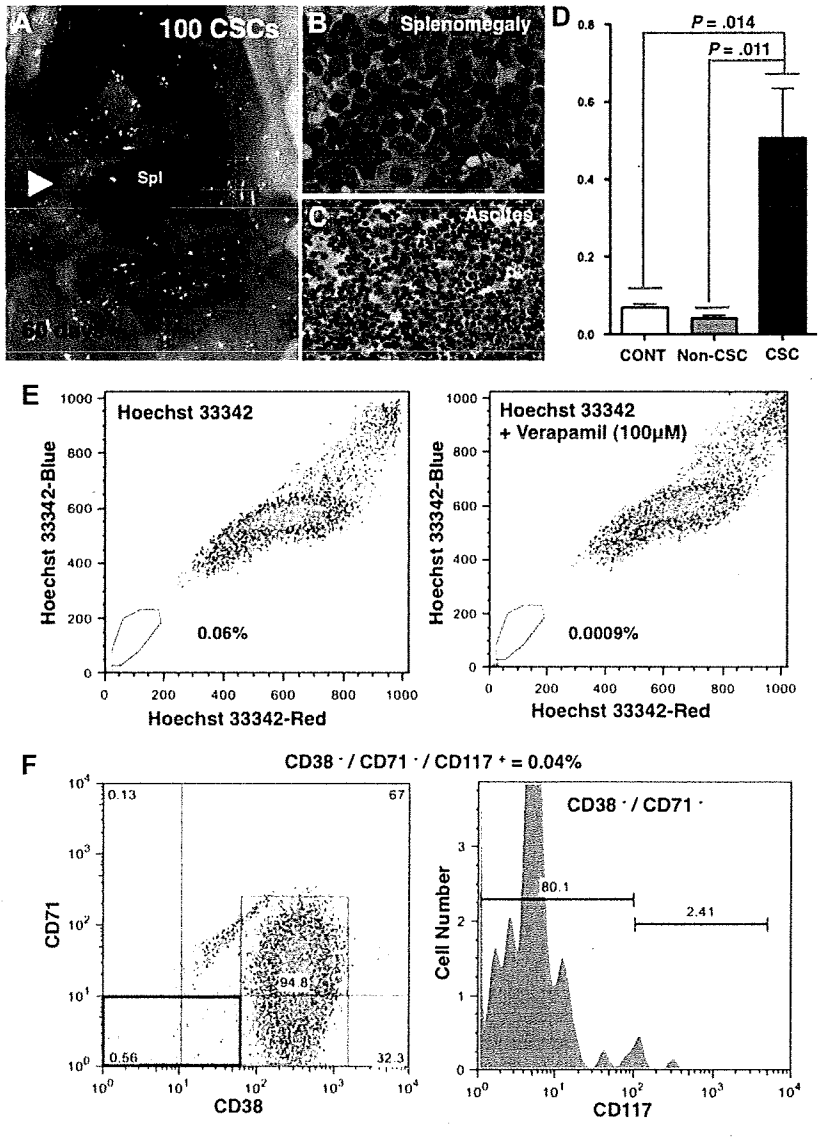

Figure 4. Regenerative potential of ATL-like lymphoma in 10^2 CSCs. ATL-like lymphoma-regenerative activity was assessed by the transplantation of 10^2 CSCs, the non-CSC fraction, and SLCs. (A) ATL-like lymphoma was regenerated by the transplantation of 10^2 CSCs into the NOD/SCID mouse at 60 days. (B) Marked splenomegaly was observed in the NOD/SCID recipient mice. (C) Ascites was also observed in the NOD/SCID recipient mice. (D) Total spleen weight was significantly increased only in the CSC-transplanted NOD/SCID mouse. (E) SP analysis of ATL-like lymphoma cells generated by the transplantation of 10^2 CSCs. (Left panel) The SP fraction (total = 0.066%) was present after CSC transplantation. (Right panel) The SP fraction was lost in the dot plot with treatment by 100 μM verapamil. (F) Surface marker analysis in the lymphoma cells regenerated by the 10^2 CSC transplantation. The CSC candidate cells ($CD38^-/CD71^-/CD117^+$) were also regenerated after transplantation of 10^2 CSCs.

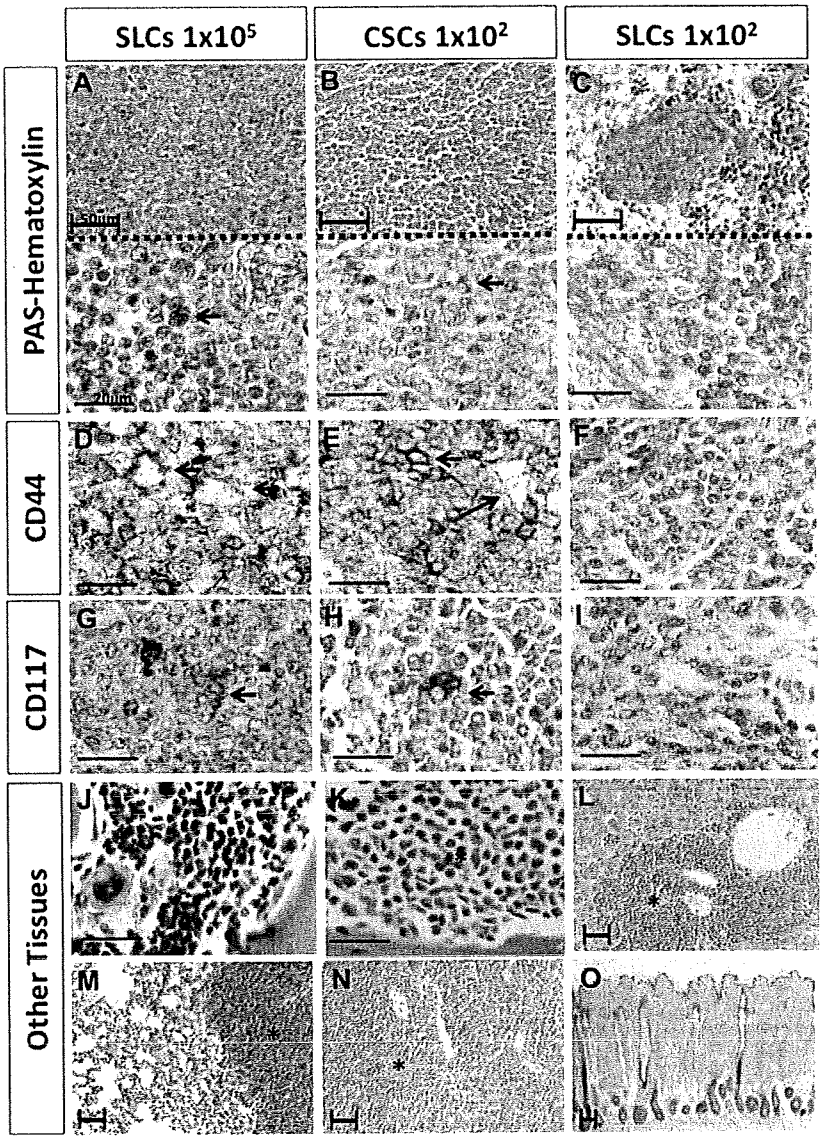

Figure 5. Histologic and immunohistochemical analyses of spleen after transplantation. At 60 days, lymphoma was regenerated after the transplantation of 10^5 SLCs and 10^2 CSCs. No lymphoma was observed after the transplantation of 10^2 non-CSCs. (A) PAS-hematoxylin staining in the 10^5 SLCs recipient spleen. (Top panel) Low magnification. (Bottom panel) High magnification. Strong PAS$^+$-stained cells were observed (←). (B) PAS-hematoxylin staining in the 1×10^2 CSCs recipient spleen. (C) PAS-hematoxylin staining in the 1×10^2 non-CSCs recipient spleen. No strong PAS$^+$ staining cells were evident. (D-I) Immunohistochemistry of CD44 and CD117, shown in the 10^5 SLC recipient spleen (D,G), in the 10^2 CSC recipient spleen (E,H), and in the 1×10^2 SLC recipient spleen (F,I). CD44 and CD117 expression is detected in the lymphoma in the spleen after 1×10^5 SLC and 1×10^2 CSC transplantation. (J) Hematoxylin and eosin (H&E) staining of the normal NOD/SCID mouse BM. Various types of blood cells, including megakaryocytes and erythroid cells, were evident. (K) Hematoxylin and eosin staining of lymphoma reconstituted in the NOD/SCID mouse BM. The BM tissue was uniformly filled with ATL-like lymphomatous cells. (L) Infiltration of lymphomatous cells was also observed in the liver. (M) Infiltration of lymphomatous cells in lung. (N) Infiltration of lymphomatous cells in lymph nodes. (O) Infiltration of lymphomatous cells was not observed in the epidermal tissues. *Lymphomatous cells. (Closed scale bar, 50 μm; open scale bar, 20 μm.)

spleen (data not shown). Interestingly, CD44 strongly positive cells were identified only in the lymphomatous spleen (Figure 5D-E) and not in the nonlymphomatous spleen (Figure 5F). Moreover, CD117$^+$ cells serving as a surrogate CSC marker were identified only in the lymphomatous spleen (Figure 5G-H) and not in the nonlymphomatous spleen (Figure 5I).

To confirm the infiltration of lymphomatous cells in other tissues, we next performed histologic analysis on BM, liver, lung, lymph node, and epidermal tissues. In the BM, as expected, various types of blood cells, including megakaryocytes and erythroid cells, were observed in WT NOD/SCID BM (Figure 5J). However, ATL-like lymphomatous cells uniformly filled in the BM of transplanted animals (Figure 5K). In addition to the BM, lymphomatous cells were also observed in the liver (Figure 5L), lung (Figure 5M), and lymph node (Figure 5N). Infiltration of lymphomatous cells was not observed in the epidermal tissues (Figure 5O).

Identification of lymphomatous cells in BM

We performed cell surface analysis of the BM mononuclear cells isolated from NOD/SCID mouse, after transplantation with 10^5 SLCs. CD38$^-$/CD71$^-$/CD117$^+$ cells (0.05%) could also be detected in BM (Figure 6A). Although, in the normal NOD/SCID mouse BM, CD3$^+$ cells were rare (Figure 6B), in contrast, almost all cells in the transplanted NOD/SCID mice were CD3$^+$ (Figure 6C).

In normal hematopoiesis, HSCs are located in specific microenvironments (niches) that also play a role in maintaining stem cell function. The osteoblastic niche in the trabecular bone and vascular niche in the medullary region are important for both the maintenance of hematopoietic[20] and leukemic stem cell function. To identify the niches of the CSCs in the BM, we performed CD117 staining as a surrogate CSC marker. Notably, CD117$^+$ cells were located both in the osteoblastic niche region (Figure 6D) in the trabecular bone and vascular niche in the medullary region (Figure 6E).

Molecular characterization and Tax expression in CSCs

To identify specific molecular markers in CSCs, we performed real-time PCR analysis on isolated CSC and non-CSC fractions (Figure 7). Recently, several molecules have been indentified as

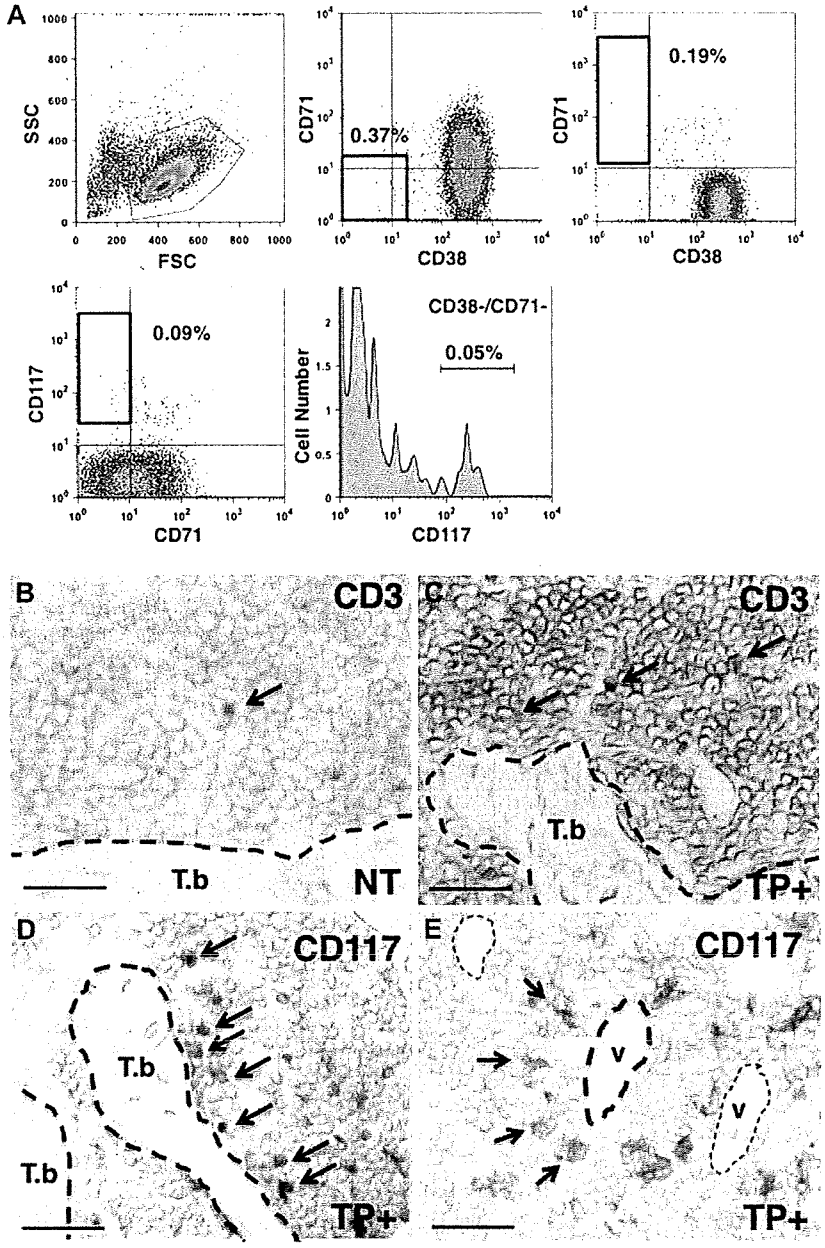

Figure 6. Flow cytometric analysis of lymphomatous cells in the NOD/SCID BM. NOD/SCID repopulating lymphomatous cells were isolated from BM. (A) Triple staining analysis with CD38, CD71, and CD117 in the BM SLCs. As was observed in spleen, the CSC candidates were also observed in the BM. (B) Histologic analysis of ATL-like lymphomatous cells in the NOD/SCID BM. In the normal NOD/SCID BM, $CD3^+$ cells were a rare population (↔). (C) In the reconstituted NOD/SCID mouse BM, $CD3^+$ cells were readily identified (arrow). (D) $CD117^+$ cells as a surrogate CSC marker could be detected in the osteoblastic niche of the trabecular bone (arrow). (E) In the medullary region, $CD117^+$ cells (CSCs) were also detected in the vascular niche (↔). T.b. indicates endosteal region in the trabecular bone; V, vascular zone; TP+, transplantation; and NT, no transplantation. Scale bar represents 20 μm.

being associated with tumor progression. Several embryonic stem cell markers have been shown to be associated with osteosarcoma[30] and bladder cancer,[31] and several HSC markers were found to be associated with leukemia development.[32] We examined *Notch1*, *CD44*, *Oct-4*, *Nanog*, *Rex1*, *Bmi1*, *SCL/tal-1*, *Flt3*, *N-cadherin*, and viral *Tax* expression in the CSCs. A total of 5×10^3 CSCs and non-CSCs were isolated by fluorescence-activated cell sorter (FACS) for RNA isolation and cDNA synthesis. These amplified cDNA were initially validated by *CD117* expression (Figure 6A). The expression level of *CD117* in the CSCs was higher than in the non-CSC fraction. In contrast, expression of *HTLV-1 Tax* mRNA was extremely low compared with the non-CSC fraction. Although expression of *CD44* in the CSC was higher than in the non-CSC fraction, *Notch1* and *Bmi-1* expression was lower than in the non-CSCs (Figure 6B). No differences were observed in *Rex1*, *Flt3*, *SCL/tal-1*, *N-cadherin*, *Oct-4*, and *Nanog* expression (data not shown).

Discussion

In this study, we have successfully identified a candidate CSC population in a mouse model of ATL, which has been shown to exhibit many of the clinical, pathologic, and immunologic features of human disease. It has been clearly established that CSCs are a specific and minor cell population, which have the potential for self-renewal, differentiation, aggressive proliferation, and chemotherapy resistance and can successfully regenerate the original malignancy when transplanted into immunocompromised mice.[14] In hematologic malignancies, several CSC candidates have been identified in acute myeloid leukemia,[12] chronic myeloid leukemia,[13] and acute lymphoblastic leukemia (ALL). Recently, Cox et al have characterized different CSC populations in ALL, which

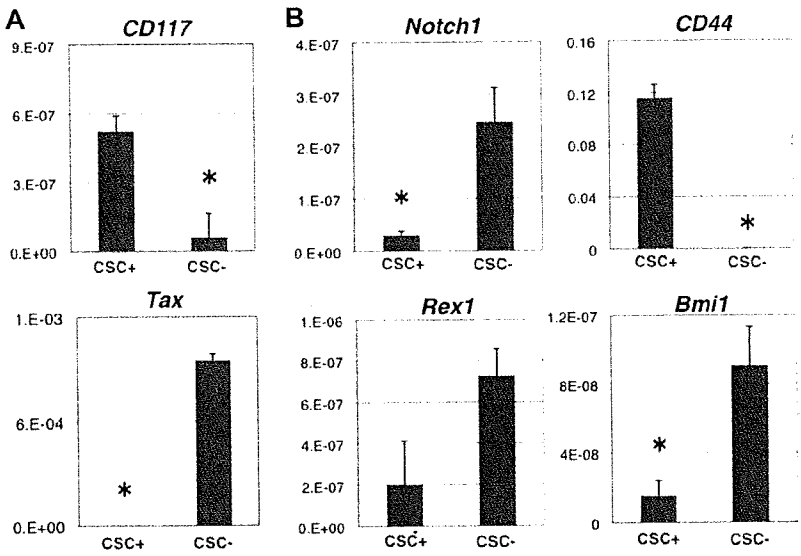

Figure 7. Molecular characterization of the CSCs and non-CSC fraction. FACS-sorted 5000 CSCs and non-CSCs were used to purify RNA and synthesize cDNA. Gene expression level was determined relative to *β-actin*. (A) *CD117* expression was used to evaluate the efficacy of cell sorting. (Top panel) *CD117* expression was higher in the CSCs than in the non-CSCs. (Bottom panel) Tax gene expression was not detected in CSCs. (B) *Notch1* and *Bmi1* expression was down-regulated in CSCs. *CD44* expression was up-regulated in CSCs. No difference was observed in the expression of the other genes, *Rex1*, *Flt3*, *SCL/tal-1*, *N-cadherin*, *Oct-4*, and *Nanog* in the CSCs and non-CSC fraction. $^*P < .05$ (significant).

include the phenotype $CD34^+/CD10^-$ or $CD34^+/CD19^-$ subpopulations in B-ALL and $CD34^+/CD4^-$ or $CD34^+/CD7^-$ subpopulations in childhood T-ALL.[33,34] Although it has been suggested that leukemic transformation occurs in a committed T- and B-cell lineage,[35] both of these candidates express the hematopoietic progenitor marker CD34, suggesting that T- and B-cell leukemia may have arisen in an early hematopoietic precursor.

ATL is a lymphoproliferative disorder caused by infection with HTLV-1.[1] Although various chemotherapeutic regimens have provided significant initial complete remission rates, most treated patients relapse, and these observations have suggested the existence of drug-resistance CSCs in aggressive disease. In this study, we have, for the first time, successfully identified and enriched a candidate CSC population in an ATL model mouse using SP analysis in conjunction with cell surface marker identification by flow cytometry. The candidate CSCs identified by their SP phenotype, which were found to overlap with a $CD38^-/CD71^-/CD117^+$ population, could regenerate the original lymphoma/leukemia with the expected phenotype when transplanted in SCID/NOD mice.

Recently, Kayo et al reported the existence of SP cells in several cultured ATL cell lines, which were defined by efficient efflux of Hoechst 33342 dye.[36] However, in these studies, both SP cells and non-SP cells could reconstitute both SP and main population cells, suggesting that SP cells in the cell lines had no specific CSC-like function in vitro.[36] The reasons for this are unclear but may well reflect changes in the cell populations as a result of culture. It has also been reported that CD90 may be a useful marker to identify CSCs in ATL cell lines. CD90 (Thy-1) is a hematopoietic progenitor marker, which is not expressed in mature T cells. In our experiments, CD90 expression was detected in approximately 1.5% of SLCs; however, expression was not associated with the CSCs. These disparate results may again reflect the differences between our transgenic and SCID/NOD animal models and ATL cell lines, which may have changed during culture.

CSCs, especially in the hematologic malignancies, share many properties with HSCs, and indeed almost all CSCs are thought to be derived from HSCs.[32] Although It has been shown that human ATL is a leukemia that, in most cases, is derived from $CD4^+$ mature T cells,[3] others exhibit a phenotype of cells at early stages in T-cell development. In our Tax transgenic mouse model, it has been shown that the ATL-like lymphoma cells were derived from an immature pre-T cell (DN2), which expresses cytoplasmic CD3, and surface CD25 and CD44.[8] In the present study, we could clearly demonstrate that the $CD38^-/CD71^-/CD117^+/CD44^+$ fraction have lymphoma and leukemia-initiating potential and proliferation activity, and have markers expressed in hematopoietic progenitor cells (CLP; common lymphoid progenitor) or Pro-T cells (DN1; double negative). CD117 (also known as c-kit) is useful marker for identifying long-term and short-term repopulating HSCs. Recently, it has shown that CD117 and its ligand stem cell factor also have important roles in early T-cell development,[37] and Notch1 with IL-7 induced differentiation of early progenitors with lymphoid and myeloid properties (EPLM) into T-cell lineage is dependent on CD117 signaling.[38] In addition to CD44, CD117 expression and the SCF/CD117 signaling pathway are also required to initiate the development of several lymphocyte populations.[39] *Notch1* is expressed in long-term HSCs and regulates the self-renewal activity of long-term HSCs in the osteoblastic niche via *Nocth1* receptor ligand *Jagged1*.[40] However, in the T-cell commitment process, whether activation of *Notch1* signaling occurs before or after EPLMs enter the thymus is still controversial.[41] In our experiments, *Notch1* expression in CSCs was down-regulated compared with the non-CSC fraction, suggesting that CSCs were derived from the EPLM or hematopoietic progenitor cells and that activation of Notch1 may be required to induce T-cell lymphoma and leukemia. It has been shown that a mutation (t(7;9) translocation) and constitutive activation of *Notch1* are frequently observed in T-ALL.[42] Whether activation of NOTCH1 signaling and in our animal model or indeed in ATL patients is related to HTLV-1 infection and Tax expression is still unclear and remains to be investigated. However, our data suggest and support the view that, at least in our mouse model, the T-cell lymphoma and leukemia-initiating stem cell is derived from an HTLV-1–infected EPLM or early hematopoietic progenitor cell and suggest that CD44 and CD117, if present, in human ATL CSCs could be possible therapeutic targets for treatment of aggressive disease.

It has been suggested that HTLV-1–derived Tax gene expression plays a key role in the development of ATL and particularly in the early stages of cell proliferation and transformation. Paradoxically, Tax gene expression is either undetectable or only at very low levels in fresh uncultured human ATL cells. In our Tax-transgenic

mouse model, Tax gene expression was also expressed at very low levels only being detected by sensitive reverse-transcription RT-PCR assays. In the present study, we found a significant further down-regulation of Tax gene in the CSCs compared with cells in the non-CSC fraction. These data support our hypothesis that CSCs are derived from EPLM or early pro-T cells (so-called DN1), as the *Lck* promoter will drive partially from DN2 and completely from the DN3 stages.[43] Recent studies have also shown that HTLV-1 can infect HSCs,[6] and lentiviral-mediated expression of Tax gene in human $CD34^+/CD38^-$ cells resulted in G_0/G_1 cell-cycle arrest by P21 and P27 up-regulation and the suppression of multilineage hematopoietic differentiation.[44] These results would suggest that the reacquisition of stem cell properties in T cell–committed progenitors might require both *Tax* expression and *CD117* and *Notch1* reexpression.

In the quantitative real-time PCR analysis, contrary to our expectations, we found a strong down-regulation of *Bmi1* in CSCs, which has been shown to be involved in the progression of several malignancies.[27] Recently, Miyazaki et al[45] reported that *Bmi1* is required for the survival, the activation of pre-T cell, and the transition from DN to double-positive cells. Although expression of *Bmi1* was detected in DN-stage, dependent up-regulation of *Bmi1* was observed from DN2 to DN4.[45] These data support our proposal that the CSCs were derived from EPLMs, but the mechanism of *Bmi1* activation in these cells remains to be investigated.

At present, the microenvironment of CSCs has not been clearly identified. Recently, Ishikawa et al reported that acute myeloid leukemia leukemic stem cells engraft within osteoblastic niche of the BM, and it has been suggested that this may afford protection from chemotherapy-induced apoptosis.[46] In the present study, we have identified potential BM niches for our candidate CSCs in the NOD/SCID model. Specifically, we found that CSCs were located both in the osteoblastic and vascular niches, but further studies are required to determine whether the former localization might also contribute to resistance to chemotherapy in our CSCs, and this is currently under investigation.

In conclusion, our transgenic and NOD/SCID animal studies have allowed the identification of candidate CSCs in this model of ATL. We think that our investigations will both inform and provide a basis for similar studies on human disease to determine whether these or equivalent stem cell populations exist and have the same characteristics. If successful, this will potentially allow the development of new anti-CSC therapeutics, which may provide more effective treatment for human disease.

Acknowledgments

The authors thank Dr Toshiki Watanabe for his critical reading of the manuscript.

This work was supported in part by the Grant-in-Aid for Scientific Research of Ministry of Education, Culture, Sports, Science and Technology, Japan (no.18790669). H.H. was supported by the Japan Society for the Promotion of Science (JSPS: Grants-in-Aid for Scientific Research), the Ministry of Health, Labor and Welfare Japan, and the Takeda Science Foundation.

Authorship

Contribution: J.Y., T.M., and I.H. designed the research; J.Y. performed the majority of FACS and transplantation analysis; T.M. performed the histologic studies, analyzed the data, and wrote the paper; K.T. assisted with cell sorting and transplantation experiments; M.K. performed the quantitative PCR experiments; H.M. and A.M. also performed experiments; Y.A. assisted with the NOD/SCID mouse experiments; H.H. and W.W.H. produced the Tax transgenic mice, developed the NOD/SCID model; and wrote the paper; and H.T. and K.Y. were involved in the design of the research.

Conflict-of-interest disclosure: The authors declare no competing financial interests.

Correspondence: Isao Hamaguchi, Department of Safety Research on Blood and Biological Products, National Institute of Infectious Diseases 4-7-1, Gakuen, Musashimurayama, Tokyo, 208-0011, Japan; e-mail: 130hama@nih.go.jp.

References

1. Yamaguchi K. Human T-lymphotropic virus type I in Japan. *Lancet.* 1994;343(8891):213-216.
2. Proietti FA, Carneiro-Proietti AB, Catalan-Soares BC, Murphy EL. Global epidemiology of HTLV-I infection and associated diseases. *Oncogene.* 2005;24(39):6058-6068.
3. Shimoyama M. Diagnostic criteria and classification of clinical subtypes of adult T-cell leukaemia-lymphoma: a report from the Lymphoma Study Group (1984-87). *Br J Haematol.* 1991;79(3):428-437.
4. Yamada Y, Kamihira S, Amagasaki T, et al. Adult T cell leukemia with atypical surface phenotypes: clinical correlation. *J Clin Oncol.* 1985;3(6):782-788.
5. Karube K, Ohshima K, Tsuchiya T, et al. Expression of FoxP3, a key molecule in CD4CD25 regulatory T cells, in adult T-cell leukaemia/lymphoma cells. *Br J Haematol.* 2004;126(1):81-84.
6. Feuer G, Fraser JK, Zack JA, Lee F, Feuer R, Chen IS. Human T-cell leukemia virus infection of human hematopoietic progenitor cells: maintenance of virus infection during differentiation in vitro and in vivo. *J Virol.* 1996;70(6):4038-4044.
7. Matsuoka M, Jeang KT. Human T-cell leukaemia virus type 1 (HTLV-1) infectivity and cellular transformation. *Nat Rev Cancer.* 2007;7(4):270-280.
8. Hasegawa H, Sawa H, Lewis MJ, et al. Thymus-derived leukemia-lymphoma in mice transgenic for the Tax gene of human T-lymphotropic virus type I. *Nat Med.* 2006;12(4):466-472.
9. Ohsugi T, Kumasaka T, Okada S, Urano T. The Tax protein of HTLV-1 promotes oncogenesis in not only immature T cells but also mature T cells. *Nat Med.* 2007;13(5):527-528.
10. Yamada Y, Tomonaga M, Fukuda H, et al. A new G-CSF-supported combination chemotherapy, LSG15, for adult T-cell leukaemia-lymphoma: Japan Clinical Oncology Group Study 9303. *Br J Haematol.* 2001;113(2):375-382.
11. Mahieux R, Hermine O. In vivo and in vitro treatment of HTLV-1 and HTLV-2 infected cells with arsenic trioxide and interferon-alpha. *Leuk Lymphoma.* 2005;46(3):347-355.
12. Jordan CT. Unique molecular and cellular features of acute myelogenous leukemia stem cells. *Leukemia.* 2002;16(4):559-562.
13. Holyoake TL, Jiang X, Drummond MW, Eaves AC, Eaves CJ. Elucidating critical mechanisms of deregulated stem cell turnover in the chronic phase of chronic myeloid leukemia. *Leukemia.* 2002;16(4):549-558.
14. Al-Hajj M, Clarke MF. Self-renewal and solid tumor stem cells. *Oncogene.* 2004;23(43):7274-7282.
15. Clarke MF. A self-renewal assay for cancer stem cells. *Cancer Chemother Pharmacol.* 2005; 56[Suppl 1]:64-68.
16. Tang C, Ang BT, Pervaiz S. Cancer stem cell: target for anti-cancer therapy. *FASEB J.* 2007; 21(14):3777-3785.
17. Goodell MA, Brose K, Paradis G, Conner AS, Mulligan RC. Isolation and functional properties of murine hematopoietic stem cells that are replicating in vivo. *J Exp Med.* 1996;183(4):1797-1806.
18. Takemori N, Hirai K, Onodera R, Saito N, Kamiguchi K, Namiki M. Vacuolated glycogen-laden leukemic cells in a case of crisis type chronic adult T-cell leukemia. *Leuk Lymphoma.* 1993;11(3):309-314.
19. Hamaguchi I, Imai J, Momose H, et al. Two vaccine toxicity-related genes Agp and Hpx could prove useful for pertussis vaccine safety control. *Vaccine.* 2007;25(17):3355-3364.

20. Mizukami T, Kuramitsu M, Takizawa K, et al. Identification of transcripts commonly expressed in both hematopoietic and germ-line stem cells. *Stem Cells Dev.* 2008;17(1):67-80.
21. Kohno T, Yamada Y, Akamatsu N, et al. Possible origin of adult T-cell leukemia/lymphoma cells from human T lymphotropic virus type-1-infected regulatory T cells. *Cancer Sci.* 2005;96(8):527-533.
22. Baba H, Yamada Y, Mori N, et al. Multiple gamma-receptor expression in adult T-cell leukemia. *Eur J Haematol.* 2002;68(6):362-369.
23. Bonnet D, Dick JE. Human acute myeloid leukemia is organized as a hierarchy that originates from a primitive hematopoietic cell. *Nat Med.* 1997;3(7):730-737.
24. Okada S, Nakauchi H, Nagayoshi K, Nishikawa S, Miura Y, Suda T. In vivo and in vitro stem cell function of c-kit- and Sca-1-positive murine hematopoietic cells. *Blood.* 1992;80(12):3044-3050.
25. Singh SK, Hawkins C, Clarke ID, et al. Identification of human brain tumour initiating cells. *Nature.* 2004;432(7015):396-401.
26. O'Brien CA, Pollett A, Gallinger S, Dick JE. A human colon cancer cell capable of initiating tumour growth in immunodeficient mice. *Nature.* 2007; 445(7123):106-110.
27. Lee CJ, Dosch J, Simeone DM. Pancreatic cancer stem cells. *J Clin Oncol.* 2008;26(17):2806-2812.
28. Lam WK, Watkins DN. Lung cancer: future directions. *Respirology.* 2007;12(4):471-477.
29. Hadnagy A, Gaboury L, Beaulieu R, Balicki D. SP analysis may be used to identify cancer stem cell populations. *Exp Cell Res.* 2006;312(19):3701-3710.
30. Gibbs CP, Kukekov VG, Reith JD, et al. Stem-like cells in bone sarcomas: implications for tumorigenesis. *Neoplasia.* 2005;7(11):967-976.
31. Atlasi Y, Mowla SJ, Ziaee SA, Bahrami AR. OCT-4, an embryonic stem cell marker, is highly expressed in bladder cancer. *Int J Cancer.* 2007; 120(7):1598-1602.
32. Savona M, Talpaz M. Getting to the stem of chronic myeloid leukaemia. *Nat Rev Cancer.* 2008;8(5):341-350.
33. Cox CV, Evely RS, Oakhill A, Pamphilon DH, Goulden NJ, Blair A. Characterization of acute lymphoblastic leukemia progenitor cells. *Blood.* 2004;104(9):2919-2925.
34. Cox CV, Martin HM, Kearns PR, Virgo P, Evely RS, Blair A. Characterization of a progenitor cell population in childhood T-cell acute lymphoblastic leukemia. *Blood.* 2007;109(2):674-682.
35. Plasschaert SL, Kamps WA, Vellenga E, de Vries EG, de Bont ES. Prognosis in childhood and adult acute lymphoblastic leukaemia: a question of maturation? *Cancer Treat Rev.* 2004;30(1):37-51.
36. Kayo H, Yamazaki H, Nishida H, Dang NH, Morimoto C. Stem cell properties and the side population cells as a target for interferon-alpha in adult T-cell leukemia/lymphoma. *Biochem Biophys Res Commun.* 2007;364(4):808-814.
37. Massa S, Balciunaite G, Ceredig R, Rolink AG. Critical role for c-kit (CD117) in T cell lineage commitment and early thymocyte development in vitro. *Eur J Immunol.* 2006;36(3):508-511.
38. Agosti V, Corbacioglu S, Ehlers I, et al. Critical role for Kit-mediated Src kinase but not PI 3-kinase signaling in pro T and pro B cell development. *J Exp Med.* 2004;199(6):867-878.
39. Parrott JA, Kim G, Skinner MK. Expression and action of kit ligand/stem cell factor in normal human and bovine ovarian surface epithelium and ovarian cancer. *Biol Reprod.* 2000;62(6):1600-1609.
40. Stier S, Cheng T, Dombkowski D, Carlesso N, Scadden DT. Notch1 activation increases hematopoietic stem cell self-renewal in vivo and favors lymphoid over myeloid lineage outcome. *Blood.* 2002;99(7):2369-2378.
41. Radtke F, Wilson A, Mancini SJ, MacDonald HR. Notch regulation of lymphocyte development and function. *Nat Immunol.* 2004;5(3):247-253.
42. Weng AP, Ferrando AA, Lee W, et al. Activating mutations of NOTCH1 in human T cell acute lymphoblastic leukemia. *Science.* 2004;306(5694): 269-271.
43. Masuda K, Kakugawa K, Nakayama T, Minato N, Katsura Y, Kawamoto H. T cell lineage determination precedes the initiation of TCR beta gene rearrangement. *J Immunol.* 2007;179(6):3699-3706.
44. Tripp A, Liu Y, Sieburg M, Montalbano J, Wrzesinski S, Feuer G. Human T-cell leukemia virus type 1 tax oncoprotein suppression of multilineage hematopoiesis of CD34+ cells in vitro. *J Virol.* 2003;77(22):12152-12164.
45. Miyazaki M, Miyazaki K, Itoi M, et al. Thymocyte proliferation induced by pre-T cell receptor signaling is maintained through polycomb gene product Bmi-1-mediated Cdkn2a repression. *Immunity.* 2008;28(2):231-245.
46. Ishikawa F, Yoshida S, Saito Y, et al. Chemotherapy-resistant human AML stem cells home to and engraft within the bone-marrow endosteal region. *Nat Biotechnol.* 2007;25(11): 1315-1321.

Inhibition of the SDF-1α–CXCR4 axis by the CXCR4 antagonist AMD3100 suppresses the migration of cultured cells from ATL patients and murine lymphoblastoid cells from HTLV-I *Tax* transgenic mice

Akira Kawaguchi,[1-3] Yasuko Orba,[1,3] Takashi Kimura,[1] Hidekatsu Iha,[4] Masao Ogata,[5] Takahiro Tsuji,[2] Akira Ainai,[2,6] Tetsutaro Sata,[2] Takashi Okamoto,[7] William W. Hall,[8] Hirofumi Sawa,[1,3] and Hideki Hasegawa[2,6]

[1]Department of Molecular Pathobiology, Research Center for Zoonosis Control, Hokkaido University, Hokkaido, Japan; [2]Department of Pathology, National Institute of Infectious Diseases, Tokyo, Japan; [3]Global COE Program, Hokkaido University, Hokkaido, Japan; [4]Department of Infectious Diseases, Oita University Faculty of Medicine, Oita, Japan; [5]Blood Transfusion Center, Oita University Hospital, Oita, Japan; [6]Center for Influenza Virus Research, National Institute of Infectious Diseases, Tokyo, Japan; [7]Department of Molecular and Cellular Biology, Nagoya City University Graduate School of Medical Sciences, Nagoya City, Japan; and [8]Centre for Research in Infectious Diseases, University College Dublin, Dublin, Ireland

Adult T-cell leukemia (ATL) is a T-cell malignancy caused by human T lymphotropic virus type I, and presents as an aggressive leukemia with characteristic widespread leukemic cell infiltration into visceral organs and skin. The molecular mechanisms associated with leukemic cell infiltration are poorly understood. We have used mouse models of ATL to investigate the role of chemokines in this process. Transfer of splenic lymphomatous cells from transgenic to SCID mice reproduces a leukemia and lymphoma that is histologically identical to human disease. It could be shown that lymphomatous cells exhibit specific chemotactic activity in response to stromal cell–derived factor-1α (SDF-1α). Lymphomatous cells exhibited surface expression of CXCR4, the specific receptor of SDF-1α. AMD3100, a CXCR4 antagonist, was found to inhibit both SDF-1α–induced migration and phosphorylation of extracellular signal-related kinase 1/2. Investigation of cultured cells from human ATL patients revealed identical findings. Using the SCID mouse model, it could be demonstrated that AMD3100 inhibited infiltration of lymphomatous cells into liver and lung tissues in vivo. These results demonstrate the involvement of the SDF-1α/CXCR4 interaction as one mechanism of leukemic cell migration and this may provide a novel target as part of combination therapy for ATL. (Blood. 2009;114: 2961-2968)

Introduction

Adult T-cell leukemia (ATL) is a peripheral T-cell malignancy caused by infection by human T lymphotropic virus type I (HTLV-I). This hematologic neoplasm develops in 1% to 5% of people infected with HTLV-I usually 2 to 4 decades after infection. A characteristic manifestation of ATL is extensive infiltration of leukemic cells into various organs, including lymph nodes, liver, spleen, lungs, and skin.[1,2] Tissue infiltration likely reflects certain unique biologic properties of the leukemic cells, and although these are poorly understood they may be related to the expression and function of chemokines, chemokine receptors,[3-7] adhesion molecules,[8,9] and resulting adhesive interactions with endothelial cells.

Chemokines are a group of structurally related cytokines that induce directed migration of various leukocyte populations.[10] Chemokine receptors are coupled to heterotrimeric G proteins and induce cell movement toward a concentration gradient of the cognate chemokine ligand.[11] Chemokines are essential for the migration and tissue localization of various lymphocyte subpopulations expressing specific chemokine receptors. Human stromal cell–derived factor-1α (SDF-1α), also known as CXCL12, binds and signals solely though chemokine receptor CXCR4.[12] CXCR4 is central to stem cell localization, serving as a chemoattractant for lymphocytes in vitro and in vivo.[13] In addition, a recent study demonstrated that the CXCR4 signal pathway may play a role in the metastasis of breast cancer cells by inducing chemotactic and invasive responses.[14]

Human ATL cells have been shown to produce several chemokines, including macrophage inflammatory protein 1α (MIP-1α),[3] MIP-3α,[4] MIP-1β,[5] I-309,[6] thymus- and activation-regulated chemokine (TARC), and macrophage-derived chemokine (MDC),[7] and express the chemokine receptors CCR4,[15] CCR5,[16] CCR7,[17] and CCR9,[18] and it has been suggested that some of these may be involved in ATL cell migration and infiltration.

Recently, we have established a model of ATL by generating HTLV-I *Tax* transgenic mice with a restriction of transgene expression to developing thymocytes.[19] These mice developed aggressive leukemic and lymphoma with a characteristic histologic phenotype showing extensive perivascular infiltration of leukemia cells into spleen, liver, kidney, lung, lymph nodes, and skin. Flow cytometric analyses demonstrated that the cells were $CD4^-$ and $CD8^-$, but positive for both CD44 and cytoplasmic CD3 indicative of a thymus-derived pre–T-cell phenotype. Cells also expressed high levels of activation markers including CD25. Lymphomatous cells from these transgenic mice could reproduce identical disease after intraperitoneal injection into SCID mice. In this study, we have used the SCID mouse model to investigate molecular mechanisms associated with leukemic cell infiltration, and have focused on the chemotactic activity of the lymphomatous cells. We

Submitted November 12, 2008; accepted June 22, 2009. Prepublished online as *Blood* First Edition paper, August 5, 2009; DOI 10.1182/blood-2008-11-189308.

The online version of this article contains a data supplement.

The publication costs of this article were defrayed in part by page charge payment. Therefore, and solely to indicate this fact, this article is hereby marked "advertisement" in accordance with 18 USC section 1734.

Table 1. Clinical and laboratory characteristics of ATL patients

Case	Date of collection	Age/sex	Subtype at diagnosis	Date of onset	WBC ($\times 10^9$/L)	Atypical cells (%)*	LDH, IU/L (normal range)†	Serum Ca (mM)‡	Infiltrated organs
1	10/16/2007	No data	Chronic	No data	16.8	80	NE	NE	NE
2	6/9/2000	70/F	Chronic	5/22/2000	26.3	34	701 (212-410)	2.20	PB
3	5/3/2003	53/M	Acute	5/3/2003	30.9	69	1426 (212-410)	Normal	PB, S, superficial LN, LN in the abdominal cavity
4	11/17/2004	45/F	Acute	11/17/2004	65.5	83	307 (119-229)	2.65	PB, S, L, Sp
5	5/1/1998	51/M	Acute	2/20/1998	58.8	88	4979 (212-410)	2.53	PB, Sp
6	11/8/1996	36/M	Acute	11/6/1996	37.9	NE	1349 (212-410)	2.29	PB, S, superficial LN, L, Sp

NE indicates not examined; PB, peripheral blood; S, skin; L, liver; Sp, spleen; and LN, lymph nodes.
*Atypical cells were morphologically diagnosed.
†Normal range was changed in 2004.
‡Normal range: 8.2-10.2 mg/dL.

could demonstrate that not only primary murine lymphomatous cells but also human ATL cells exhibit specific chemotactic activity in response to SDF-1α and that this is associated with a specific interaction with CXCR4 and activation of extracellular signal-related kinase 1/2 (ERK1/2) signaling. It could also be shown that AMD3100, a specific CXCR4 antagonist,[20] markedly inhibited cell migration and phosphorylation of ERK1/2 by SDF-1α in both murine and human cells. In addition, AMD3100 inhibited infiltration of lymphomatous cells into liver and lung tissues in SCID mice. These results have identified a novel molecular mechanism associated with leukemic cell migration and provide a framework for designing new therapeutic strategies for the treatment of ATL.

Methods

Cells

Tumor cells from spleens of HTLV-I *Tax*-transgenic mice, in which normal splenocytes were replaced with lymphomatous cells, were isolated using a Lymphoprep kit (Axis-Shield ProC As), and suspended in RPMI 1640 medium. Thereafter, lymphomatous cells (10^6/mL) were intraperitoneally injected into SCID mice. At 28 days after injection, tumor cells were again isolated from ascites and spleens of the injected SCID mice. The isolated tumor cells from SCID mice (primary murine lymphoblastoid [pML] cells) were harvested and kept frozen until use. The pML cells were cultured in RPMI 1640 medium supplemented with 10% fetal bovine serum (FBS; Hyclone), antibiotics, and 2 mM L-glutamine, and maintained at 37°C in 5% CO_2 and investigated after 1 or 2 days in culture. As a control, T cells were isolated from spleens of C57BL/6 mice with a Pan T-cell Isolation Kit (Miltenyi Biotec). Isolated control T cells were cultured in the same conditions as that of pML cells. Leukemic cells from ATL patients who were diagnosed on the basis of characteristic clinical features and laboratory findings were isolated by Ficoll-Hypaque gradient centrifugation and kept frozen until use. The cells were cultured for 2 days in RPMI 1640 medium supplemented with 20% FBS (Equitech-Bio), antibiotics, 2 mM L-glutamine, and 1 ng/mL interleukin-2 (IL-2; Peprotech EC), and maintained at 37°C in 5% CO_2. Isolated cells contained more than 90% leukemic cells at the time of analysis. The clinical and laboratory characteristics of ATL patients are shown in Table 1.

All animal experiments were approved by the Animal Care and Use Committee of the Hokkaido University School of Medicine and the Animal Care and Use Committee of the National Institute of Infectious Diseases. Tumor cells from ATL patients were maintained in RPMI 1640 medium supplemented with 15% FBS (Equitech-Bio), penicillin G (50 U/mL), and streptomycin (50 μg/mL:Sigma-Aldrich). Ethical permission for use of patient-derived cells and pathologic materials was approved by the Ethical Committee of the Oita University Faculty of Medicine and informed consent was obtained in accordance with the Declaration of Helsinki.

Antibodies and chemicals

Antibodies for phosphorylated forms of p44/42 mitogen-activated protein kinase, Akt, p38, phosphatidylinositol 3 kinase (PI3K), and IκB, and total forms of p44/42 mitogen-activated protein kinase, Akt, and IκB were obtained from Cell Signaling Technology. Anti–mouse/human CXC-chemokine receptor 4 (CXCR4/CD184) polyclonal antibody was purchased from eBioscience. Recombinant mouse thymus and activation regulated chemokine (TARC/CCL17), macrophage inflammatory protein 3α (MIP-3α/CCL20), recombinant murine and human stromal cell–derived factor-1α (SDF-1α/CXCL12) were purchased from Peprotech EC. Recombinant murine regulated on activation normal T expressed and secreted (RANTES/CCL5) and cutaneous T cell–attracting chemokine (CTACK/CCL27) were purchased from Aeris Antibodies. Recombinant mouse secondary lymphoid-tissue chemokine (SLC/Exodus-2) was purchased from Chemicon International. The CXCR4 antagonist, AMD3100 octahydrochloride, was purchased from Sigma-Aldrich. Mitogen-activated protein kinase (MEK) inhibitor, U0126, was purchased from Promega. All recombinant chemokines and antagonists were dissolved in distilled water, and U0126 was dissolved in dimethyl sulfoxide. For immunohistochemical staining, monoclonal antihuman/mouse CXCL12/SDF-1 antibody (1:100; R&D Systems) was used.

Immunoblotting

pML cells were serum-starved for 2 hours, and then lysates from 10^6 cells per sample were prepared after stimulation with SDF-1α (100 ng/mL) at the indicated time points. Protein content was determined using a Pierce BCA Protein Assay kit. Equal amounts of protein were separated by polyacrylamide gel electrophoresis and transferred onto polyvinylidene difluoride membranes (Immobilon-P; Millipore).

Chemotaxis assay

For cells from both ATL patients and pML cells, the migration efficiency of cells was assessed using 5-μm-pore Transwell filter membranes (Kurabo). For each membrane filter, 5×10^6 cells were cultured in 200 μL RPMI 1640 containing 0.5% bovine albumin. The membrane insert was placed in the well of the 24-well plate that contained 500 μL RPMI medium with murine recombinant chemokine the noted concentrations, and incubated at 37°C for 2.5 hours. After removal of filter inserts, the number of cells that had migrated from the upper chamber to the lower well was counted using a hemocytometer viewed under a microscope. Chemokines used in the assays are as described in "Antibodies and chemicals." To examine the effect of antagonists on SDF-1α–induced chemotactic activity, cells were incubated with antagonists for 1 hour and then loaded in the upper chamber. Migrated cells were counted using a hemocytometer. The effect of SDF-1α on cell survival was measured by assays of viability at 24 or 48 hours.

Flow cytometry

For quantification of cell-surface CXCR4 receptor expression, pML cells were incubated for 30 minutes with PE-conjugated rat anti–mouse-CD184/

CXCR4 monoclonal antibody (× 20; BD Pharmingen), or PE-anti–rat IgG2b (Beckman Coulter) as an isotype control. The data obtained were analyzed using Flowjo software (Tree Star).

Reverse transcription and reverse-transcription–polymerase chain reaction

Total RNA was prepared from pML cells using TRIzol reagent (Gibco-BRL). Total RNA (1 μg) was reverse-transcribed with Omniscript reverse transcriptase (QIAGEN), according to the manufacturer's instructions. Polymerase chain reaction (PCR) was carried out in a volume of 20 μL: initial denaturation at 94°C for 2 minutes was followed by 30 cycles of 94°C for 15 seconds, 58°C for 30 seconds, and 68°C for 30 seconds. As an internal control, *β-actin* was also amplified. The following primers were used: for *Tax*, 5′-AGGCAGATGAGAATGACCATGA-3′ and 5′-TTTTCACTCCCAGGCTCTAAGC-3′; for SDF-1α, 5′-CACCGATCCACACAGAGTACTTG-3′ and 5′-AGCCAACGTCAAGCATCTGA-3′; for β-actin, 5′-CTCCTTAATGTCAGCGATTTC-3′ and 5′-CAGCCGTGCAACAATCTGAA-3′. PCR products were electrophoresed in agarose gel, and visualized using a UV illuminator.

Immunohistochemistry

Tissues were fixed in neutral-buffered formalin (Sigma-Aldrich), embedded in paraffin, sectioned, and stained with hematoxylin and eosin (H&E). For immunohistochemical staining, the sections were deparaffinized with xylene and dehydrated using decreasing concentrations of ethanol. Thereafter, sections were boiled in a pressure cooker for 2 minutes in 0.01 M citrate buffer (pH 6.0) for antigen retrieval. Mouse sections were incubated with 0.3% H_2O_2 in methanol at room temperature for 15 minutes to block endogenous peroxidase. After washing with PBS, sections were pretreated with blocking solution A (Histofine; Nichirei Biosciences) at room temperature for 60 minutes. The sections were sequentially incubated with primary antibody at 4°C overnight, with blocking solution B (Nichirei Biosciences) for 10 minutes, and with universal immunoperoxidase polymer (Nichirei Biosciences) for 10 minutes. The signal was visualized with diamino-3,3′-diaminobenzidine. For human sections, slides were initially treated with peroxidase block solution (Dako) for 5 minutes, and incubated with 10% normal goat serum (Nichirei Biosciences) at room temperature for 60 minutes. The sections were incubated with primary antibody at 4°C overnight, and thereafter followed by incubation for 90 minutes with labeled polymer-HRP antimouse conjugation (Envision system; Dako) and color development using diamino-3,3′-diaminobenzidine. Tumor cells from human ATL patients were stained by the Giemsa method to confirm their morphology. To examine expression of SDF-1α in human tissues infiltrated by ATL cells, liver samples infiltrated by ATL cells from ATL cases (n = 5) were immunohistochemically examined.

AMD3100 in vivo treatment

SCID mice (6-week-old; nontreated [NT]) were inoculated intraperitoneally with AMD3100 pretreated (AMD^+) or NT pML cells (5×10^2, 5×10^3, and 5×10^4 cells/mice, n = 5 in each group). In AMD^+ group, the pML cells were incubated with 20 μg/mL AMD3100 in RPMI (0.3% fetal calf serum) at 37°C for 30 minutes as described previously.[21] The mice inoculated with AMD^+ pML cells were treated with 300 μg AMD3100 daily for 3 weeks (5 days per week) intraperitoneally (AMD-treated mice). The mice inoculated with NT pML cells were treated with PBS for 3 weeks (5 days per week) intraperitoneally (untreated mice). The mice were killed at 23 days after inoculation of pML cells. Genomic DNA of liver and lung tissues was extracted, and the copy numbers of *Tax* gene and *β-actin* gene were measured by quantitative real-time PCR using QuantiTect Probe PCR Kit (QIAGEN). The relative copy number of *Tax* was represented by the ratio to the copy number of *β-actin* gene. The primers used for detection of *Tax* genome and *β-actin* gene were as follows: Tax forward: 5′-aggcagatgacaatgaccatga-3′, Tax reverse: 5′-ttttcactcccaggctctaagc-3′, Tax probe: 5′-FAM-ccccaaatatccccggg-TAMRA-3′, and beta-actin forward: 5′-cacegatccacacagagtacttg-3′, β-actin reverse: 5′-cagtgctgtctggtggtacca-3′, and β-actin probe: 5′-FAM-cagtaatctccttctgcatcctgtcagcaa-TAMRA-3′.

Statistics

Statistical comparisons between experimental groups were analyzed using the Student *t* test, and for all comparisons a *P* value less than .05 was considered significant.

Results

Chemotactic response of pML cells to SDF-1α

Several studies have reported that human ATL cells exhibit chemotactic activity in response to the chemokines TARC, SLC, and RANTES.[7,10-12] We examined the chemotactic activity of pML cells in response to several cytokines and chemokines. Specifically, the pML cell migratory response to 6 different chemokines, TARC, MIP-3α, RANTES, SLC, CTACK, and SDF-1α, was investigated using a chemotaxis chamber assay. It could be shown that pML cells had a marked, dose-dependent chemotactic response to SDF-1α (Figure 1A). The cells also showed a weak chemotactic response to TARC and SLC, which has been reported for human ATL cells.[7,10,12] The migratory efficiencies of pML cells and control normal mouse T cells in response to SDF-1α were compared and it could be clearly shown that the migratory response of pML cells was markedly higher (Figure 1B).

We examined the effect of SDF-1α on survival of pML cells. SDF-1α had no effect on survival of pML cells after 24- and 48-hour incubation. We also investigated the effect of NF-κB inhibitor (BAY65-1942), which induces apoptosis of pML cells at

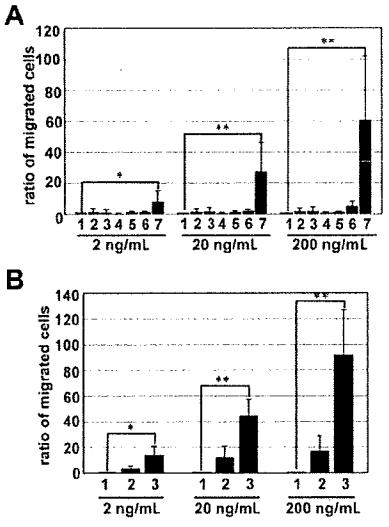

Figure 1. Chemotactic activity of pML cells in response to various chemokines. (A) Chemotactic activity of pML cells in response to chemokines SDF-1α, MIP-3α, TARC, SLC, RANTES, and CTACK. Migration efficiency of pML cells was estimated using a Transwell assay in the presence of various concentrations (2, 20, and 200 ng/mL) of chemokines. The number of migrating pML cells was counted using a hemocytometer viewed under a microscope. The results are expressed as the fold number of the untreated control pML cells. The number below each bar corresponds to each chemokine: 1, control; 2, TARC; 3, LARC; 4, RANTES; 5, CTACK; 6, SLC; and 7, SDF-1α. These results were confirmed by 3 independent experiments. The data are presented as mean values ± SD. $^*P < .05$. $^{**}P < .01$. (B) Chemotactic activity of pML cells and normal T cells. The number of migrating cells was measured as described for panel B in the presence of 0, 2, 20, and 200 ng/mL SDF-1α. The results are expressed as the fold number of the normal T cells. These results were confirmed by 3 independent experiments. The data are presented as mean values ± SD. $^*P < .05$; $^{**}P < .01$.

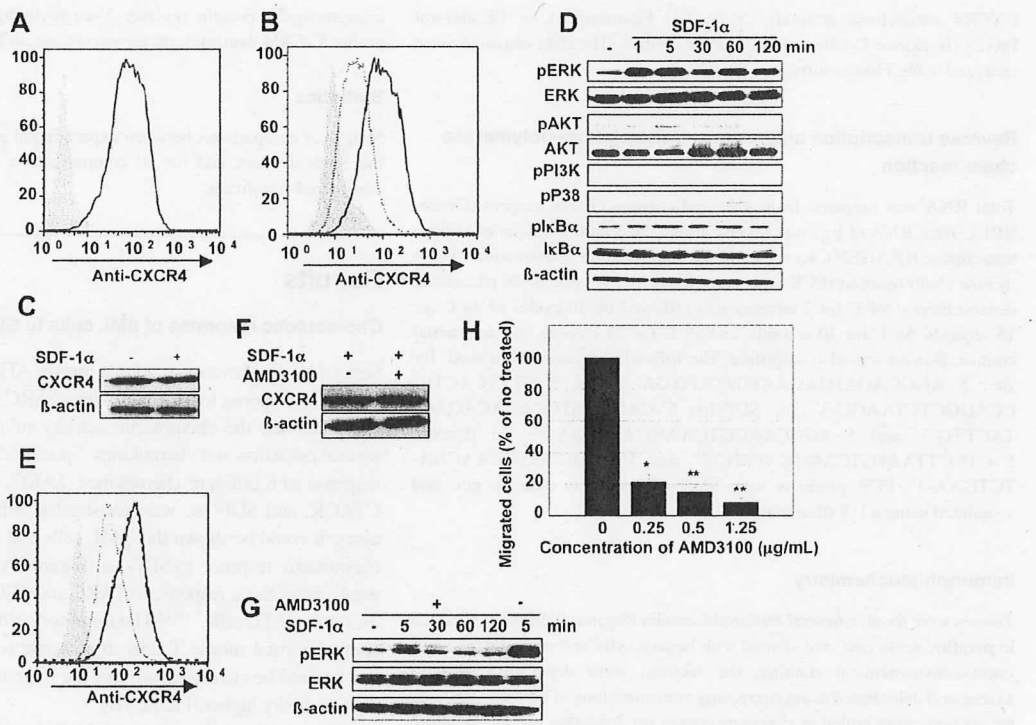

Figure 2. CXCR4 expression on the surface of pML cells and SDF-1α–induced CXCR4 translocation. (A) Flow cytometric analysis of cell-surface expression of CXCR4 in pML cells. CXCR4 was detected by incubating cells with PE-conjugated rat anti-CXCR4 antibody. Red line represents CXCR4 expression, and gray area represents the result of staining with isotype-matched control antibody. (B) CXCR4 expression on pML cell surface. Cells were treated in the presence (blue dot line) or absence (red line) of 100 ng/mL SDF-1α. After a brief wash, cells were incubated with the same antibody as used in Figure 2A. The gray area represents staining with isotype-matched control antibody. (C) Total cellular protein level of CXCR4 in the presence (+) or absence (−) of SDF-1α (100 ng/mL) for 5 minutes. (D) SDF-1α–induced phosphorylation of ERK1/2 in pML cells. pML cells were treated before lysis with 100 ng/mL SDF-1α for the indicated times. Cell lysates were analyzed by immunoblotting analysis with anti–phospho-ERK, –total ERK, –phospho-AKT, –total AKT, –phospho-PI3K, –phospho-P38, –phospho-IκBα, –total IκBα, or –β-actin antibodies. (E) Expression levels of cellular surface CXCR4 in pML cells after treatment with AMD3100. Cells were pretreated with 25 μg/mL AMD3100 for 1 hour, and then stimulated with SDF-1α for 5 minutes (black dot line). Cells were also stimulated exclusively with SDF-1α (blue dot line) or were untreated (red line). The gray area represents staining with isotype-matched control antibody. (F) Expression of total CXCR4 protein with (+) or without (−) AMD3100 treatment. The lysates from treated cells were analyzed by immunoblotting with anti–mouse/human CXCR4 polyclonal antibody. (G) Phosphorylation of ERK1/2 in pML cells with or without AMD3100 treatment. After pretreatment with AMD3100 (25 μg/mL) for 1 hour, cells were stimulated with SDF-1α for the indicated times (0, 5, 30, 60, and 120 minutes). The cellular lysates were analyzed by immunoblotting. In the lane at the right, the cells received no AMD3100 treatment but were stimulated with SDF-1α. (H) Migration assay of pML cells using AMD3100 at various concentrations (0, 0.25, 0.5, and 1.25 μg/mL). pML cells were preincubated for 60 minutes with AMD3100 at the indicated concentrations, and then subjected to the migration assay in the presence of 100 ng/mL SDF-1α. The data were presented as a relative ratio of migrating cells: the number of migrated cells in the presence of AMD3100/the number of nontreated cells. These results were confirmed by 3 independent experiments. The data are presented as mean values ± SD. $^*P < .05$. $^{**}P < .01$.

24 hours after incubation, to determine whether SDF-1α might reverse this. More than 80% of the pML cells were dead at 24 hours after incubation with BAY65-1942, and it could be clearly shown that SDF-1α could not reverse the effect of the inhibitor and permit the survival of the pML cells (supplemental Figure 1, available on the *Blood* website; see the Supplemental Materials link at the top of the online article).

Cell surface localization of CXCR4 in pML cells

Flow cytometry analysis was used to examine expression of CXCR4, which is the specific receptor for SDF-1α on pML cells, and it could be shown that CXCR4 was localized on the cell surface (Figure 2A). Chemokine binding to their cell surface receptors is known to lead to internalization of the receptor-ligand complex, with subsequent activation of intracellular signal cascades.[22] To investigate the effect of SDF-1α on CXCR4 expression, we analyzed CXCR4 localization after treatment with SDF-1α (100 ng/mL). It could be demonstrated that treatment with SDF-1α down-regulated CXCR4 surface expression (Figure 2B). Total expression levels of CXCR4 protein were unaffected (Figure 2C), demonstrating that cell surface CXCR4 in pML cells was internalized upon exposure to SDF-1α.

Intracellular signal pathways regulated by SDF-1α/CXCR4 in pML cells

SDF-1α is known to activate the ERK1/2 pathway. ERK1/2 is a downstream effector of the MEK-dependent signaling cascade, and the MEK-ERK pathway is an important mediator of chemotaxis in many cell types.[23,24] To confirm whether SDF-1α treatment activates the MEK-ERK pathway in pML cells, we initially examined phosphorylation of ERK1/2. Immunoblotting with phospho-ERK antibody revealed that SDF-1α treatment led to a rapid activation of ERK1/2 (Figure 2D), with phosphorylation of ERK1/2 evident within 1 minute and peaking at 5 minutes after SDF-1α exposure. This was sustained at least until 120 minutes. No significant changes were observed in total ERK protein expression over this time period (Figure 2D). These results were consistent with a previous study in which SDF-1α was shown to promote internalization of CXCR4 and activation of ERK1/2 in multiple myeloma cells.[25] Phosphorylation of ERK1/2 was found to be abrogated by the MEK inhibitor U0126, even in the presence of SDF-1α (supplemental Figure 2A), and about 40% decrease in the migration of pML cells was observed in chemotaxis assays (supplemental Figure 2B). To further analyze CXCR4/SDF-1α–mediated intracellular signaling, we investigated whether SDF-1α

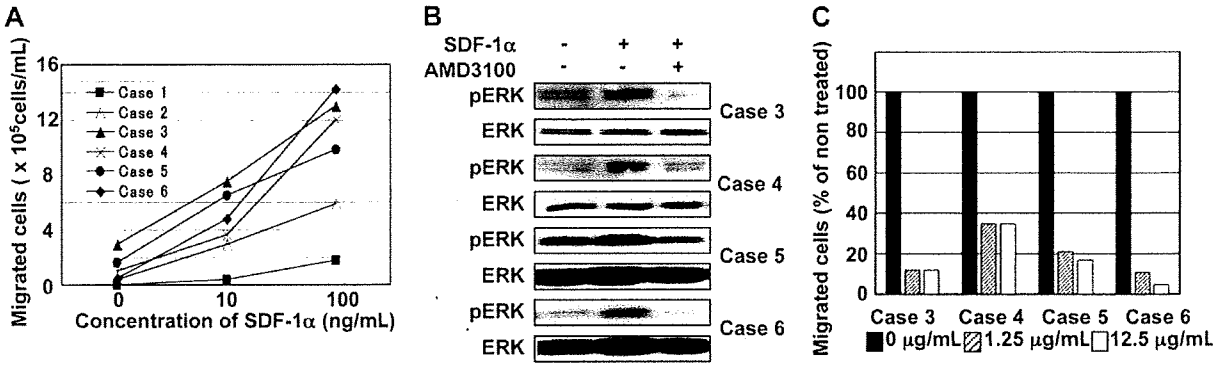

Figure 3. Chemotaxis of human ATL cells in response to SDF-1α. (A) The migration assay of human ATL cells freshly prepared from frozen stocks of ATL patient's peripheral blood mononuclear cells and cultured for 2 days. Human ATL cells were also examined for chemotactic activity in response to SDF-1α, using recombinant human SDF-1α. After incubation with SDF-1α for 2.5 hours, the number of the cells migrating to the lower chamber was counted using a hemocytometer. (B) Phosphorylation of ERK1/2 after stimulation with SDF-1α (100 ng/mL for 5 minutes) in human ATL cells with or without AMD3100 pretreatment (25 μg/mL for 1 hour). (C) The inhibitory effect of AMD3100 on the migration of human ATL cells. Human ATL cells were preincubated for 60 minutes with the indicated concentrations of AMD3100, and then applied to the migration assay in the presence of 100 ng/mL SDF-1α. The number of the migrating cells was counted, and represented in the bar graph as a relative ratio of migrated to nontreated cells.

activated other molecules downstream of CXCR4. In contrast to ERK1/2, phosphorylation of several other molecules, including PI3K, Akt, p38, and IκBα, was not significantly affected (Figure 2D). These results demonstrate that SDF-1α exclusively activates the MEK-ERK pathway in pML cells.

Effects of the CXCR4 antagonist AMD3100 in pML cells

We investigated the effect of the selective CXCR4 antagonist AMD3100 on chemotaxis and ERK1/2 signaling. As previously shown, CXCR4 surface expression was down-regulated by SDF-1α treatment (100 ng/mL); however, this inhibition was abrogated by AMD3100 treatment (25 μg/mL; Figure 2E). Total levels of CXCR4 protein expression were unchanged by AMD3100 treatment (Figure 2F). We also examined whether AMD3100 affects phosphorylation of ERK1/2, and it could be demonstrated that phosphorylation was markedly decreased (Figure 2D,G). SDF-1α–induced migration activity of pML cells was assayed in the presence of AMD3100 and compared with untreated cells, and migration was found to be inhibited 79% and 91.2% in the presence of 0.25 and 1.25 μg/mL AMD3100, respectively (Figure 2H). These results show that AMD3100 inhibits the migration of pML cells in a dose-dependent manner by inhibiting the MEK-ERK pathway downstream of CXCR4-SDF-1α.

Chemotaxis of cells derived from ATL patients in response to SDF-1α

To determine whether the results of our mouse model accurately reflected human disease, we analyzed chemotactic activity of leukemic cells from 6 ATL patients after short-term culture (2 days) in response to SDF-1α. Clinical and laboratory information relating to the patients is summarized in Table 1. Phenotypic analysis of the leukemic cells showed that all cell populations were $CD4^+/CD25^+$, and Giemsa staining clearly demonstrated typical features of ATL with cells having enlarged nuclei, often with lobulation, compared with normal peripheral blood lymphocytes (data not shown). All of the ATL cells exhibited chemotaxis in response to SDF-1α treatment in a dose-dependent manner (Figure 3A). In addition, immunoblotting revealed that SDF-1α–induced phosphorylation of ERK1/2 occurred in 4 of the 6 ATL cases examined (Figure 3B); immunoblotting studies in the 2 remaining cases could not be carried out due to insufficient amounts of cell lysates. AMD3100 treatment of the human ATL cells strongly blocked phosphorylation of ERK1/2 (Figure 3B) and abrogated cell migration (Figure 3C). These results clearly demonstrate involvement of the SDF-1α/CXCR4-ERK pathway in human ATL cell migration, and the inhibitory potential of AMD3100.

SDF-1α expression in tissues

SDF-1α is constitutively expressed in numerous tissues in mice.[26] We confirmed expression of SDF-1α mRNA in various organs, including brain, heart, lung, liver, spleen, and kidney. However, we were unable to demonstrate a positive signal for SDF-1α mRNA expression in pML cells (Figure 4A). To examine the presence of SDF-1α protein, we used 2 different antibodies for tissue analysis, and could detect positive signals using a monoclonal anti-CXCL12/SDF-1 antibody. Weak immunopositive signals for SDF-1α protein were observed in epithelial cells of mouse liver hepatic ducts (Figure 4B-C); no positive signals were observed in control experiments that used normal mouse IgG instead of primary antibody (data not shown). In HTLV-I *Tax* transgenic mice, leukemic cell infiltration was readily observed in areas surrounding the SDF-1α–immunopositive hepatic ducts (Figure 4D-E).

In ATL patients, SDF-1α–immunopositive signals were readily detected in the epithelial cells of hepatic ducts that were surrounded by infiltrating leukemic cells. (Figure 4F-G). We also observed SDF-1α immunostaining in epithelial cells of regenerative hepatic ducts in regions infiltrated by leukemic cells (Figure 4H-I). Infiltrating cells were also detected in the portal triad region, and again specifically around the hepatic ducts where epithelial cells were positive for SDF-1α (Figure 4F-I). We also performed immunostaining with anti–SDF-1α antibody of control disease-free human liver samples, and immunopositive staining was also detected in hepatic duct epithelial cells (Figure 4J-K).

Inhibition of pML cell invasion by AMD3100 in vivo

We performed in vivo experiments to determine whether AMD3100 could inhibit leukemic cell invasion in SCID mice. The mice were inoculated intraperitoneally with AMD3100 pretreated (AMD^+) or nontreated (NT) pML cells (5×10^2, 5×10^3, and 5×10^4 cells/mice, $n = 5$ in each group). The mice inoculated with AMD^+ pML cells were treated with AMD3100 (AMD-treated mice), and control mice inoculated with NT pML

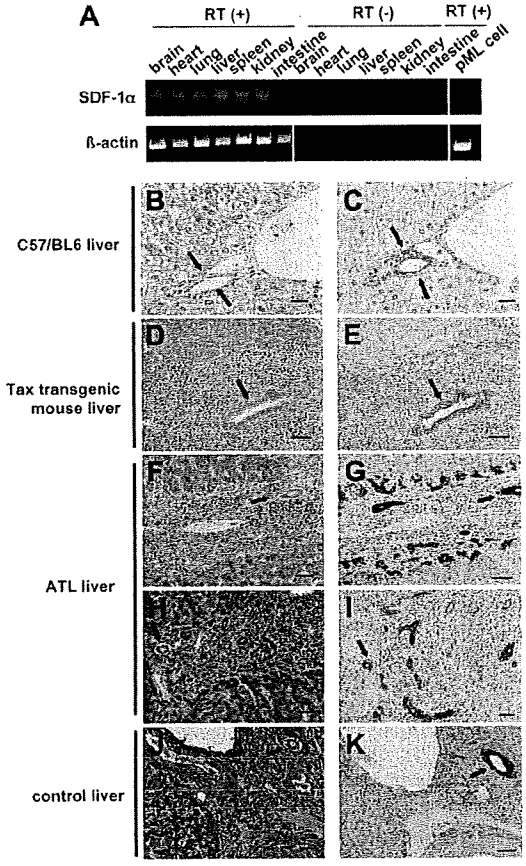

Figure 4. Tissue expression of SDF-1α. (A) The expression levels of SDF-1α transcripts in various tissues of C57BL/6 mice, including brain, heart, lung, liver, spleen, kidney, and intestine with or without reverse transcriptase (RT) reaction. In the lane at the right, the expression level of SDF-1α transcripts in pML cells was also examined. β-Actin was used as an internal control. Vertical lines have been inserted to indicate a repositioned gel lane. (B-K) Immunohistochemical analysis of SDF-1α protein. H&E staining (B,D) and immunostaining (C,E) of SDF-1α in bile ducts from a normal C57BL/6 mouse (B-C) and in a bile duct surrounded by infiltrating tumor cells from a HTLV-I *Tax* transgenic mouse (D-E). Black arrows indicate the same bile duct in serial sections for panels B and C and panels D and E. Bars indicate (B-C) 20 μm or (D-E) 50 μm. Immunohistochemical analysis of SDF-1α protein in liver bile ducts from ATL patients (F-I) and a patient without ATL (J-K). Serial sections of H&E-stained liver from ATL patients (F,H) were examined with immunostaining using anti–SDF-1α antibody (G,I). Black arrows indicate the same bile duct in serial sections for panels F and G and panels H and I. Serial sections of (J) H&E-stained liver from a patient without ATL were also analyzed for (K) SDF-1α expression. Black arrows indicate serial sections of the same bile ducts for panels J and K. Bars indicate 50 μm. Brown indicates immunopositive reaction (C,E,G,I,K).

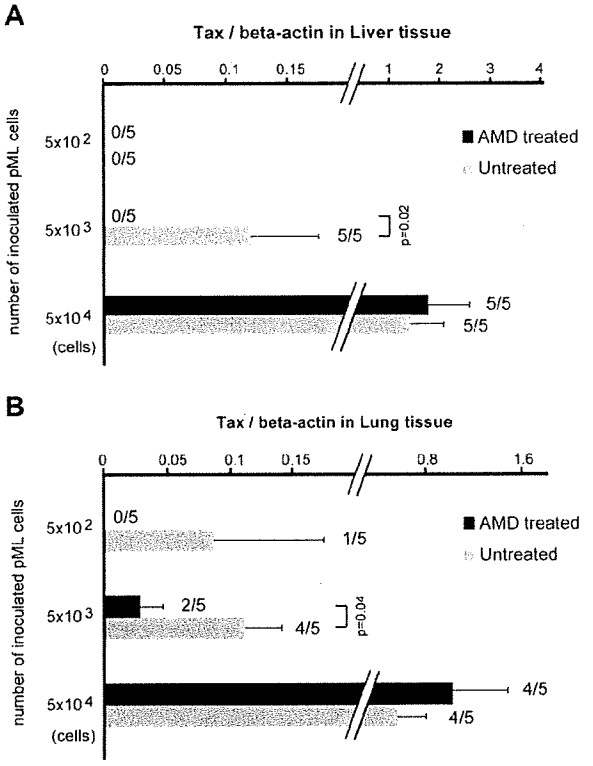

Figure 5. Inhibition of pML cell invasion by AMD3100 in vivo. Infiltration of pML cells to the liver (A) and lung (B) was inhibited by AMD3100 treatment. SCID mice inoculated with pML cells (5×10^2, 5×10^3, and 5×10^4 cells/mice) were treated with either AMD3100 (AMD treated) or PBS (untreated) for 3 weeks (5 times per week) through intraperitoneal injection. Infiltration of pML cells that contain the HTLV-I *Tax* gene into liver and lung tissues was examined using quantitative real-time PCR. The relative copy number of *Tax* genome of the group (inoculated with 5×10^2, 5×10^3, and 5×10^4 pML cells) was represented by the ratio to the copy number of β-actin in liver (A) and lung (B) tissues. The ratio of *Tax*-positive mice/total number of mice was represented on the right side of each bar (mean ± SE).

cells were treated with PBS (untreated mice) for 3 weeks (5 times per week) through intraperitoneal injection. The mice were killed at 23 days after pML cell inoculation. Invasion of pML cells containing the HTLV-I *Tax* gene into liver and lung tissues was examined using quantitative real-time PCR. The relative copy number of *Tax* was represented by the ratio to the copy number of β-actin (Figure 5). In the pML cell–inoculated group (5×10^2), the *Tax* gene was not detected in the liver of either AMD-treated or untreated mice (n = 5 in each group), whereas *Tax* was exclusively detected in one lung tissue of 5 untreated mice (Figure 5). When the mice were inoculated with 5×10^3 pML cells, the ratio of *Tax* genome to *β-actin* gene was significantly inhibited in AMD-treated mice in both liver and lung tissues compared with untreated mice. Furthermore, *Tax* was detected in all of the untreated mice (n = 5), whereas this was not detected in any of the AMD-treated mice (n = 5, Figure 5). No significant differences were observed between AMD-treated and untreated mice (n = 5, in each group) that were inoculated with 5×10^4 pML cells (Figure 5). Thus, CXCR4/SDF-1α plays a key role in migration of ATL cells in vivo and AMD3100 inhibits infiltration of pML cells into liver and lung. The results also show that the inhibitory effect of AMD3100 on tissue infiltration of pML cells is influenced by the numbers of inoculated pML cells.

Discussion

Patients with aggressive ATL characteristically display symptoms of leukemic cell infiltration in multiple organs including skin, bone marrow, spleen, liver, lung, and brain. However, the mechanisms of ATL cell infiltration are poorly understood. Chemokines are small secretory proteins that control migration and activation of leukocytes and other types of cells through interaction with a group of 7-transmembrane-domain G protein–coupled receptors (GPCRs). It is known that chemokines may also promote cellular growth and survival and have been associated with metastasis in several malignancies. Specifically it has been shown that breast cancer cells express CXCR4, and high concentrations of SDF-1α are typically present at metastatic sites of breast cancer.[14] The interaction between SDF-1α and CXCR4 has also been implicated in bone metastasis in prostate cancer.[27]